World Electric Vehicle Journal

MDPI

Article

Impact of Unidirectional Charging, Vehicle-to-Everything and Battery Energy Storage System on a Microgrid Incorporating Demand Side Management and Variable Renewable Energy

Muhammad Ahsan Ali [1,*], Muhammad Ali [1] and Ali Raza [1,*]

[1] Department of Electrical Engineering, University of Engineering and Technology, 54890 Lahore, Pakistan; m.ali@uet.edu.pk

* Correspondence: shmahsanali@gmail.com (M.A.A.); a.raza@uet.edu.pk (A.R.)

Abstract

Electric vehicles are being upgraded to support Vehicle-to-Everything charging, moving beyond the currently prevalent unidirectional Grid-to-Vehicle charging. This necessitates comparing their impact on the grid. Very little work is currently available to quantitatively compare these three cases. Moreover, conventional models related to power system analysis are used in these studies. This changed regime of electric vehicle incorporation in microgrids now requires a modular model where attributes of any microgrid constituent entity can be changed independently. Consequently, Agent-Based Modelling is chosen to perform this analysis. This study first develops an analytical framework using parametrized models of constituent nodes of an isolated microgrid. Then various grid performance aspects are quantitatively evaluated in the cases of (i) electric vehicles with unidirectional charging, (ii) electric vehicles with a Vehicle-to-Everything charging feature and (iii) an equivalent-sized stationary Battery Energy Storage System without electric vehicles. Such grid performance aspects include reliability, curtailment, and non-dispatchability of electric supply. This study concludes that Vehicle-to-Everything offers benefits, though marginally, over unidirectional charging for all three considered grid performance aspects. Similarly, a stationary Battery Energy Storage System offers benefits, though marginally, over Vehicle-to-Everything for all three grid performance parameters. It concludes that the Battery Energy Storage System size requirement in a microgrid is reduced by roughly the equivalent aggregated size of batteries in the same system with Vehicle-to-Everything charging-enabled electric vehicles. This study shows (ii) results in 0.0012%, 0.0600% and 0.0067% improvements over (i) and (iii) results in 0.0050%, 0.0724% and 0.0100% improvements over (i) in reliability, curtailment and non-dispatchability, respectively, in the case of two electric vehicles. Similarly, this study shows (ii) results in 0.0002%, 0.0306% and 0.0177% improvements over (i) and (iii) results in 0.0199%, 0.0344% and 0.0177% improvements over (i) in reliability, curtailment and non-dispatchability, respectively, in the case of one electric vehicle. Further, a cost comparison in (ii) and (iii) is made. It is found that (ii) is a more cost-effective solution, based on yet-to-be-peer-reviewed market research references, than (iii) even if an electric vehicle is retrofitted for Vehicle-to-Everything charging.

Keywords: Battery Energy Storage System; electric vehicle; Grid-to-Vehicle; Multi-Agent System; Vehicle-to-Everything; Vehicle-to-Grid

Academic Editor: Grzegorz Sierpiński

Received: 6 October 2026
Revised: 19 November 2026
Accepted: 26 November 2026
Published: 28 November 2026

Copyright: © 2026 by the authors. Published by MDPI on behalf of the World Electric Vehicle Association. Licensee MDPI, Basel, Switzerland. This article is an open access article distributed under the terms and conditions of the Creative Commons Attribution (CC BY) license.

1. Introduction

Electric vehicle charging is being revolutionized in terms of algorithms controlling energy flow management in a microgrid. A framework for studying transformation in charging techniques requires a suitable parametrized scenario that can be configured for both Vehicle-to-Everything (V2X), Grid-To-Vehicle (G2V) charging technologies and Battery Energy Storage System (BESS). For this purpose, energy routing mechanisms in a number of studies are referenced to develop a framework most suitable for this purpose.

Several techniques for optimal energy flow in this field have been developed. In this study, network constraints and market considerations are encountered in a very limited fashion while performing energy transactions. A Multi-Agent System (MAS)-based hybrid AC-DC microgrid optimization for cost and operations using Particle Swarm Optimization (PSO) is presented in [1]. A modular fashion-based mechanism using consensus-making to optimize energy transactions in a microgrid is detailed in [2]. DC Energy Management Systems (EMSs) categorization based on microgrid planning and control is elaborated in [3]. Planning and control are also discussed in this study. Residential Direct Current (DC) microgrid EMSs are presented in [4]. EMS and control for DC microgrids are described in [5]. In [6], EMSs related to this field are discussed. Control and EMS for residential microgrids are developed in [7] from thermal and electrical aspects. A centralized MG is discussed in [8], optimized by availing an Evolutionary Algorithm (EA) in a residential MG incorporating a demand response. This EA also features minimal computational effort. An islanded cluster of MGs operated by an EMS utilizing scheduling for RES and load variances is discussed in [9]. Day-Ahead coordination and Intra-Day scheduling of an EV fleet is discussed in [10]. A data-predictive method to control dynamic optimization in a reliable islanded microgrid operation is studied in [11]. A plethora of techniques used to study an islanded microgrid are present in this highly evolving field of energy transition.

In [12], Microgrid systems are stabilized using V2G support and supercapacitors. However, inflexibility in dealing with module-based parameters of rapidly changing energy paradigms is inhibiting its efficacy for this study. A virtual power plant's optimal operation mechanism using EV ABM is explained using operational profitability in [13]. Optimizing cost and charging/discharging EVs for V2G using MAS with multi-energy generation scheduling is studied in [14] and [15]. Uncertainties in VRE, EV and V2G modes in bi-level optimization of MG scheduling are discussed in [16]. This paper discussed V2G systems involving massive electric vehicle integration and strategies to operate them. Artificial Bee Colony optimization is used for V2G, G2V and V2X in [17]. However, without the use of ABM, this optimization becomes difficult to compute for a higher number of nodes. Review papers for V2Gs and charging infrastructure are referred to in [18] and [19], respectively. They have summarized the horizon of available varieties of both in a very consolidated way. In [20], electric vehicles are reviewed regarding their trends, policies, Lithium-Ion batteries, BMSs, charging infrastructure and smart charging solutions. Stochastic optimal procedures for EV and MG management are discussed in [21]. A number of projects to explore V2G opportunities are presented in [22]. An interesting questionnaire about different aspects related to V2X conducted in Sweden is discussed in [23].

Hydrogen Energy Storage System (ESS)- and Battery Energy Storage System (BESS)-based methods incorporating distributed energy resources for cooperative model predictive control of networked microgrids are discussed in [24].

However, every study bears an analytical framework based on a few suitable boundary conditions to facilitate that analysis. It is very difficult to use a particular one among them and enhance it to solve a newly generated problem. Studying the impact of a newly introduced V2X technology, in contrast to prevalent G2V, for an islanded microgrid

https://doi.org/10.3390/wevj17120635

incorporating uncertainty of renewable energy resources optimized dynamically for DS balance is quite cumbersome. This study deals with a simplistic model of all V2X variants (e.g., V2H, V2I, V2B, V2V, etc.) by modelling them from energy management aspects only. For example, their modelling is limited to their associated battery capacity, initial and dynamic SOC, battery round-trip efficiency, line losses associated with energy handling to and from them, tariff of energy moving to and from them, C-rating of batteries associated with them, their connectivity to neighbouring nodes, etc. From now on in this study, all V2X entities will be treated as a generic node with all these aspects defined. Globally, massive BESS deployments have started. However, V2X is offering an alternative to BESS deployments by claiming that another recently developed battery management system feature of an electric vehicle, V2X, will limit the need for massive BESS deployments. This has started the debate over whether V2X can suffice for the need for BESS in limiting solar curtailment. This debate has translated into exploring quantitative comparisons of V2X versus G2V on a grid.

An isolated microgrid constitutes a number of electrical prosumers interacting independently. Such problems include electric vehicles as well. Charging technologies are rapidly evolving for such EVs. Some battery management systems feature only a unidirectional charging facility. These are referred to as G2V. Now, a new technology, V2X, is featured in battery management systems (BMSs). By V2X, it is implied that an electric vehicle's BMS features all of Vehicle-to-Vehicle (V2V), Vehicle-to-Infrastructure (V2I), Vehicle-to-Load (V2L), V2G, Vehicle-to-Home (V2H), Vehicle-to-Building (V2B), Vehicle-to-Device (V2D), etc.

Our problem is confined to a comparative study of G2V versus V2X and stationary BESS on a microgrid's overall performance aspects: reliability, non-dispatchability and curtailment.

This paper has contributed to the field in the following ways:

- Development of a framework to study the flow of energy in an isolated microgrid;
- Comparison of V2X, G2V and stationary BESS on an isolated microgrid performance; reliability, VRE curtailment, non-dispatchability;
- Sensitivity analysis of the model with respect to the number of electric vehicles;
- Cost comparison of stationary BESS versus V2X-enabled electric vehicles.

Limitations

This modelled islanded microgrid is accompanied by a number of limitations worth mentioning. It will help future researchers and analysts to consider it before applying conclusions of this study. Moreover, it will direct future research work to the relevant research gaps quickly.

Renewable energy having a uniform Gaussian distribution is assumed throughout this study. A lot of parameters can be considered to make it more and more realistic, e.g., incorporation of Time-of-Day (ToD), current weather and forecasts (clouds and their specific types, smog (and concentration of its different constituent particles, e.g., PM2.5, PM10, etc.), fog, rain, solar and lunar eclipses, temperature, wind speeds, wind direction, etc.) and current cosmic weather and its forecast (solar radiance, solar maxima/minima, etc.).

Similarly, EV battery type could be considered (e.g., Nickel-Cadmium, Lithium-Ion, Lithium Iron Phosphate (LFP), Depth-of-Discharge (DoD) variations, availability of regenerative braking, road conditions (off-road, muddy, loose soil, clay, sand, compact pavement, city road, expressway, motorway, turning radii), driving habits (acceleration and deceleration tendencies, graduality in speed change, choosing energy-efficient routes, etc.), vehicle maintenance (thermal stability of battery housing, transmission system lubrication, steering agility, etc.), charging infrastructure (in-house, in-street, distant

commercial setups, in-journey), frequency of travel, average destination distance, average number of passengers, average weight of vehicle, purpose of vehicle (ride-hailing service, backup, commute, long-distance travel, etc.)).

Grid-related parameters could be considered, e.g., average energy mix ratios, share of VREs in grid-connected supply/demand, distribution system lengths, extent of behind-the-meter energy storage batteries, extent of utility BESS already present in the grid, capacity of transmission line connecting the local grid to the national grid, etc.

Further limitations that need to be addressed for further exploration of the subject are costs related to rapidly changing design and development of modern electronics, e.g., solar panels, solar inverters, Maximum Power Point Tracking (MPPT) devices, Point of Common Coupling (PCC) devices, Home Energy Management Systems (HEMS), windmills, domestic batteries, utility stationary BESS, V2X-based vehicles, commercial charging, vehicle rentals, etc.

2. Grid Model Development Using Parametrization

Grid aspects shortlisted for the study include grid reliability, energy curtailment, and non-dispatchability. In the reviewed literature, dozens of studies are cited. These studies are based on different approaches to model or optimize energy management in a microgrid. The nature of development in technology is rapidly becoming modular. So, conventional approaches do not offer flexibility to accommodate a newly developed feature. This flexibility is achieved in the presented microgrid model using an elementary parameterization-based algorithm. This framework is developed in the paper using the following equations. Grid reliability is formulated using the definition implemented in [11] as the Energy Index of Reliability (EIR), a term for grid reliability. EIR is formulated in this paper as (1) and equivalently, (1a):

$$\text{EIR} = 1 - \frac{Expected\ Energy\ not\ served}{Total\ demanded\ energy} \quad (1)$$

or,

$$\text{EIR} = \frac{Expected\ Energy\ served}{Total\ demanded\ energy} \quad (1a)$$

In this study, "EIR" will be used interchangeably with grid reliability. Ref. [25] presents a similar model of an islanded microgrid comprising ten prosumer nodes. Reliability, non-dispatchability and curtailment parameters for its MG are used as parameters for V2X. In [26], a similar concept of resiliency index is discussed. Simulation parameters for both EVs, node 6 and node 8, are adjusted so that both these nodes imitate EVs with G2V capability only. Simulation results show better grid reliability for the MG having V2X-based EVs as compared to that with G2V. A typical microgrid model is shown in Figure 1 [27].

Each ABM node is an independent prosumer node of an isolated microgrid in Figure 2. Bus bars are indicated with arrows to direct focus on the energy trading aspects of a node only. The cost and amount of traded energy are also calculated at runtime. This cost also acts as the variable to control transactions.

https://doi.org/10.3390/wevj17120635

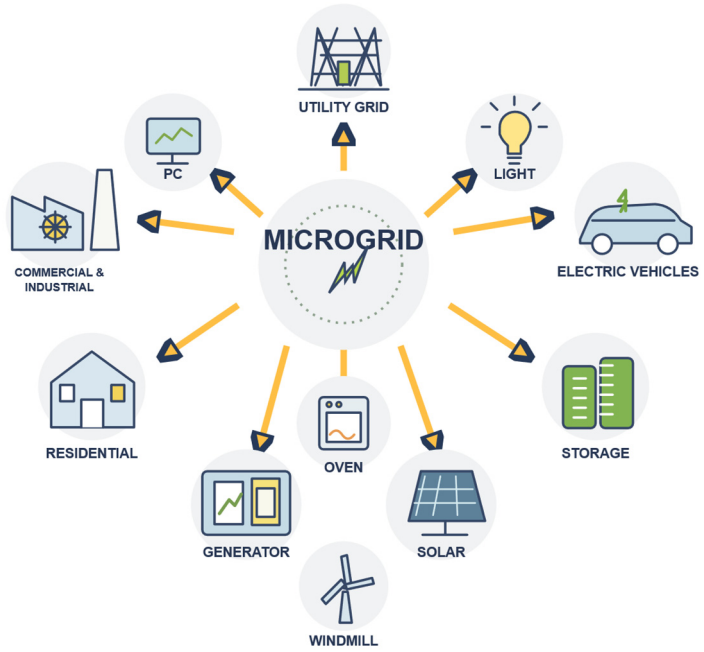

Figure 1. Schematic representation of a typical microgrid adapted for this study.

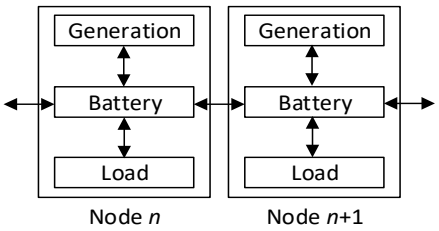

Figure 2. Agent-based model of a prosumer node in the developed grid model.

2.1. Grid Nodes Interconnectivity

An isolated microgrid comprising ten prosumer nodes is considered. Figure 3 illustrates the connectivity of the first four prosumer nodes, while Table 1 defines the connectivity of each node with its neighbouring nodes. Ten nodes are chosen as that is a typical number of main functional nodes in an isolated microgrid. Furthermore, handling complexity for ten nodes is easy in a study. However, the microgrid model is flexible enough to accommodate any number of nodes.

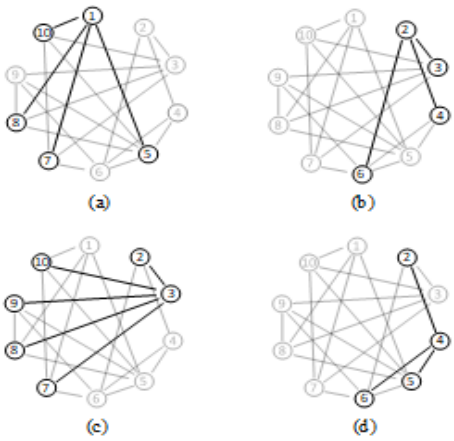

Figure 3. Graphical representation of interconnections to its connected neighbours for (**a**) Node 1, (**b**) Node 2, (**c**) Node 3 and (**d**) Node 4.

Table 1. Nodes' interconnectivity in modelled isolated microgrid.

Node	Device	1	2	3	4	5	6	7	8	9	10
1	Wind 1	1	0	0	0	1	0	1	1	0	1
2	PC	0	1	1	1	0	1	0	0	0	0
3	Fan	0	1	1	0	0	0	1	1	1	1
4	Light	0	1	0	1	1	1	0	0	0	0
5	Solar	1	0	0	1	1	1	0	1	1	1
6	EV 1	0	1	0	1	1	1	1	0	1	0
7	Gen	1	0	1	0	0	1	1	0	0	1
8	EV 2	1	0	1	0	1	0	0	1	1	0
9	Wind 2	0	0	1	0	1	1	0	1	1	0
10	Oven	1	0	1	0	1	0	1	0	0	1

2.2. Parameterized Grid Model Development

In the developed model of an isolated microgrid, electric energy is traded among different nodes after evaluating the feasibility of a prospective energy transaction. Each node records the cost of traded energy for its last five trading deals, e.g., the fifth-last traded energy unit cost is defined as r_{-5}. Similarly, r_{avg}^{n} defines the average cost of energy traded in a node during the last five transactions. It is formulated as (2)

$$r_n^{avg} = \frac{1}{5}\sum_{k=-5}^{-1} r_k \tag{2}$$

On similar grounds, r_{min}^{n}, r_{max}^{n} and r_{range}^{n} are formulated as (3–5)

$$r_n^{min} = min\,(r_{n-5}, r_{n-4}, r_{n-3}, r_{n-2}, r_{n-1}) \tag{3}$$

$$r_n^{max} = max\,(r_{n-5}, r_{n-4}, r_{n-3}, r_{n-2}, r_{n-1}) \tag{4}$$

$$r_n^{range} = r_n^{max} - r_n^{min} \tag{5}$$

Energy tradable by a node, E_n^{Δ}, is formulated as (6). This is calculated as the difference between this node's current energy level and its nominal one, i.e.,

$$E_n^{\Delta} = E_n^{curr} - E_n^{nom} \tag{6}$$

The sum of this node's energy tradable to all connected interested nodes neighbouring it is expressed as E_n^{neigh} in (7).

$$E_n^{neigh} = \sum E_r^{neigh}\ \forall\ r \in connected\ interested\ neighbours \tag{7}$$

A node "α" is defined in (8), which is a quantitative threshold to determine a node's ability to export/import energy to its connected energy importing/exporting neighbours. DS balance at a node is balanced and thus controlled using "α".

$$\alpha = \left|\frac{E_n^{neigh}}{E_n^{\Delta}}\right| \quad \text{for } E_n^{\Delta} \neq 0 \tag{8}$$

for $E_n^{\Delta} = 0$, α is not updated and, thus, not evaluated.

Curtailment of energy, e.g., in case the node is primarily a renewable energy generator and its neighbouring nodes are not interested in importing its exportable energy, is represented by C_n^{curr} formulated in (9). This represents physically wasted energy at a node. E_n^{gen} is defined as the energy generated in the nth node.

$$C_n^{curr} = E_n^{\Delta} - E_n^{neigh} + E_n^{gen} \tag{9}$$

Curtailed energy associated with a node equals the summation of exportable energy and generated energy of this node minus energy taken by its neighbouring nodes.

MG's overall accumulated wasted energy at all nodes since the start of the simulation is expressed as $C_n^{cummulative}$ *in* (10):

$$C_n^{cummulative} = C_n^{cummulative} + C_n^{curr} \quad (10)$$

$E_n^{forcasted}$ is defined to evaluate the extent of energy import/export at a node in the next ten seconds. This time is chosen so as to deal with the maximum possible revisit time for a node. This is formulated in (11):

$$E_n^{forcasted} = 10 \times L_n^{curr} \quad (11)$$

For each node, cumulative power generated since the start of the analysis is termed as P_{cum}^n. It is expressed in (12):

$$P_{cum}^n = P_{cum}^n + E_n^{\Delta} \quad (12)$$

Total energy generated by all nodes is termed as Pcum. Gn, for all nodes of this modelled microgrid, is used to represent the MG's total power since the start of analysis. It is formulated in (13).

$$P_{cum}^{gen} = \sum_N G_n \quad (13)$$

where "α" plays the basic role of achieving the DS balancing objective. Another variable "Exim" (that is used to express whether a node is a producer (Exim = 2), Prosumer (Exim = 1) or a consumer (Exim = 0) on dynamic energy profiles of a node is shown in Table 2. Fair open market trading is, thus, carried out to dictate the cost per unit of energy, quantity, and timing for each transaction during simulation.

Table 2. Decision-making thresholds for the developed algorithm for energy management optimization.

$\boldsymbol{E_n^{\Delta}}$	**1**				**0**			
α	0	$0 < \alpha < 1$	1	>1	0	$0 < \alpha < 1$	1	>1
$\boldsymbol{L_n^{curr}}$	L_n^{max}	L_n^{max}	L_n^{nom}	L_n^{min}	L_n^{min}	L_n^{min}	L_n^{nom}	L_n^{max}

2.3. Algorithm Flowchart of Energy Flow Management in Modelled Grid

An algorithm can be most concisely explained in the form of a flowchart.

2.3.1. Initialization

At the start of execution, interconnection information of all the nodes in a microgrid is fed to the algorithm. Further, a database encompassing basic profiling parameters of all nodes is initialized and passed on to the developed isolated MG model. Flowcharts are explained in Figures 4 and 5.

2.3.2. Non-Dispatchability or Curtailment (NC) Emergency Check

If a reference node faces energy non-dispatchability, i.e., if it is currently a consumer node and its neighbouring nodes cannot export to it for any reason, or energy curtailment, i.e., if it is currently a producer node and its neighbouring nodes cannot import from it for any reason, it is referred to in this work as a non-dispatchability-curtailment (NC) emergency.

2.3.3. Non-Dispatchability or Curtailment Emergency Level 2 (NC2) Check

After that, a reference node is randomly chosen. Initially, it checks whether there has been an occurrence of an NC emergency of level 2 in the last iteration of the algorithm or not. If that is the case, it measures the duration of the emergency and notes this incremental addition of emergency in the relevant statistics. Then, the tradable energy of the

reference node determines the Exim status of the same. α is determined, and the reference node is again evaluated for NC emergency. α = 80% is chosen as a reasonable threshold to define sustenance of an emergency and is used in the algorithm as the deciding threshold for NC emergency level 2. If this node is still in the state of emergency, nominal SOC levels of all neighbours of the reference node are redefined so as to take advantage of maximum possible flexibility to avoid an NC emergency. Once again, an NC check is performed on the said node. If it is still in the state of emergency, an NC emergency of level 2 is declared. Relevant statistics of non-dispatchability or curtailment are evaluated and recorded in the relevant statistics.

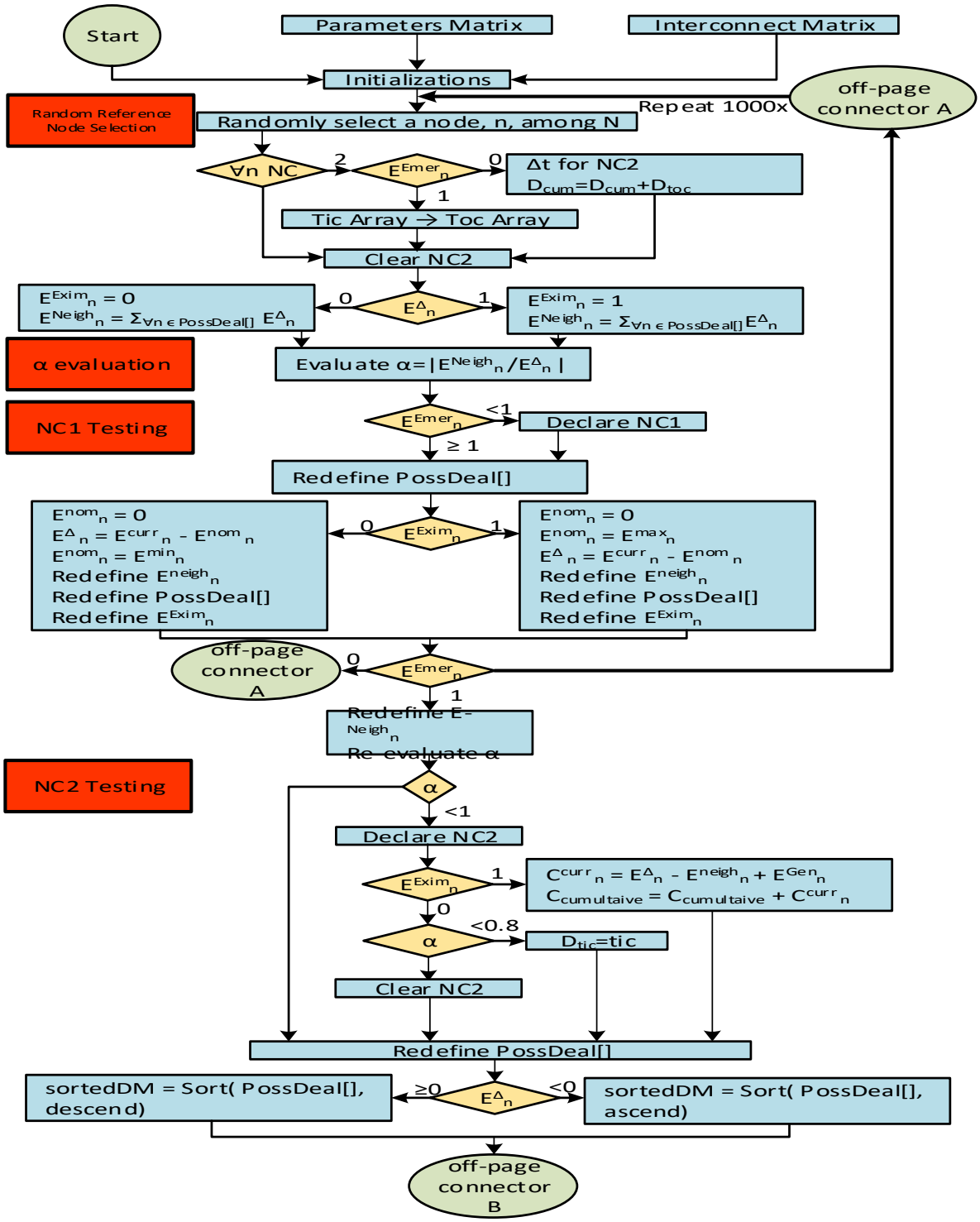

Figure 4. Energy management optimization algorithm flowchart

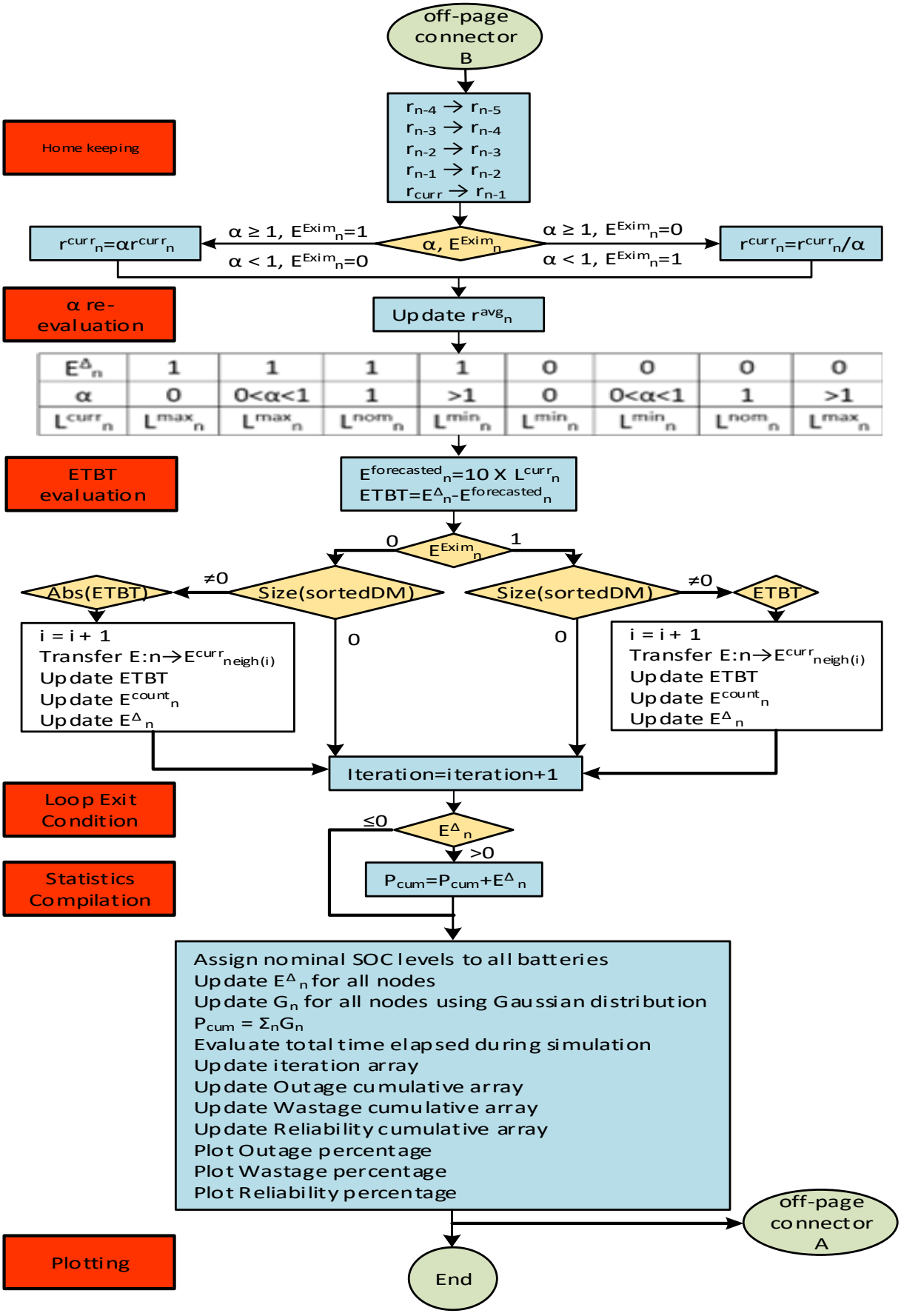

Figure 5. Energy management optimization algorithm flowchart.

2.3.4. Dynamic Definition of Interested Connected Neighbours of Reference Node

After that, a new set of interested connected neighbours is once again populated as the PossDeal array. It is then sorted in ascending or descending order depending on α and Exim (exporter or importer) status of this node. Correspondingly, rates are redefined for the node under consideration. Later, the current load level of this node is changed so as to operate it at its maximum/minimum or nominal value depending on its Exim status and the value of α. Then, the estimated energy to be transferred from the reference node is calculated keeping in view the forecasted load.

It is assumed that it will keep operating for the next ten seconds. This duration is chosen empirically; as a result of simulated iterations tens of thousands of times, it has proved to be well above the highest revisit time for a node as the reference node.

2.3.5. Energy Transfers and Housekeeping

Later, energy transfers are started from the reference node to its connected interested neighbours in the priority order defined by the PossDeal array. This energy transfer is done till the time either the PossDeal array is exhausted, or the reference node's tradeable energy is exhausted. Finally, nominal statistics and SOC levels of batteries are reallocated to all the affected nodes that have participated in the current iteration. Relevant parameters are updated as part of housekeeping. All statistics of cumulative nature are also updated before the next iteration. SOC levels are kept same for the next iteration.

2.3.6. Battery Modelling

Battery considerations, related to minimum/maximum SOC levels, charging/discharging timings, time constants, business of a prosumer node for charging/discharging are modelled. Maximum SOC for all batteries is assumed to be 100. These parameters are quantified in Table A1 that serves as the parameter input to the simulation environment.

2.3.7. Parameters for Simulation

There are forty-one parameters attributed to every node of the simulated isolated microgrid. For the sake of clarity, these parameters are listed in Table A1 in Appendix A.

2.3.8. C-Rate of Batteries

Although exact charging and discharging rates differ a lot in electric vehicles, industry averages vary around 0.1–0.3C on domestic AC chargers, while varying from 0.5 to 2 C on commercial DC fast chargers.

By C-rate, charging rate as compared to a battery's capacity is meant, e.g., for a C-rate of 1, a 50kWh battery will be charged in an hour with a continuous 50kW power. It should be kept in mind that this is the average C-rate of an EV. It can vary depending on the State-of-Health (SOH) of a battery and its current SOC. Generally, C-rate dynamically gets reduced while a battery has an SOC of 80–100, as keeping a relatively high voltage level of the destination battery while charging non-linearly becomes difficult for the charging circuit and vice versa.

In this study, a typical industry average of C-rate = 1 is chosen.

https://doi.org/10.3390/wevj17120635

2.3.9. Duty-Cycle of EVs

Very few studies have been performed to evaluate the duty cycle of cars in a city. A study for this purpose is available for the United States of America [28]. This study states that a typical US car is used for 64.6 min = 4.49% of the time. This same duty cycle of a vehicle is used as the unavailable time percentage for both EVs in the study. Caution is advised, as any such peer-reviewed study is not yet available at a large scale. So, this percentage suffers from limitations related to a particular region. This is one of the reasons that this study finds batteries in EVs a strong alternative candidate to serve the purpose of a utility stationary Battery Energy Storage System (BESS). It is evident later in the results section that EV batteries can fulfil the purpose performed by stationary BESS.

2.3.10. Line Losses

A line losses lookup table similar to that of the interconnect matrix is formed where each connected node pair is associated with a resistance value. At the time of energy transfer, current proportional to the energy transferred is squared, multiplied by the associated resistance value among the two nodes in the lookup table, and the resultant line loss is divided into half among the trading nodes and adjusted accordingly in the statistics.

2.3.11. Statistics Compilation and Plotting

At the end of a thousand iterations, cumulative results and percentages for non-dispatchability, curtailment and reliability are evaluated and plotted w.r.t. iteration number.

3. Results

Simulation is performed on an Intel 13th Generation i9 processor with 12GB RAM. The software application used is MATLAB 2026a. An islanded microgrid comprising ten nodes is used. Ten nodes are chosen as they represent an average connectivity extent in an islanded microgrid. The model starts energy transactions by applying rules developed in Section 2. The starting point of the execution is to treat any particular node as the reference node for an iteration. This node is chosen using a randomizing function. Simulations for the relevant aspects of the microgrid for both G2V, V2X and BESS scenarios are compared in this section. Each simulation is iterated a thousand times.

For the sake of sensitivity analysis, all of this study will initially be performed with two EVs and the corresponding stationary BESS, and later, this study will be performed with only one EV.

Each simulation iteration initiates with a randomly selected reference node. Multiple run-to-run simulations against the same parameters are plotted.

3.1. Grid Reliability with Two EVS

Grid reliability for G2V, V2X and stationary BESS is simulated thirty times for two EVs. Each time, a different seed but with the same sequence is chosen for all three cases.

Graphical results for reliability in the case of G2V are shown in Figure 6. Graphical results for reliability in the case of V2X are shown in Figure 7. Graphical results for reliability in the case of stationary BESS are shown in Figure 8. Figure 9 plots grid reliability for all three cases with two EVs.

Results of thirty runs for reliability in all three cases are tabulated in Table 3.

https://doi.org/10.3390/wevj17120635

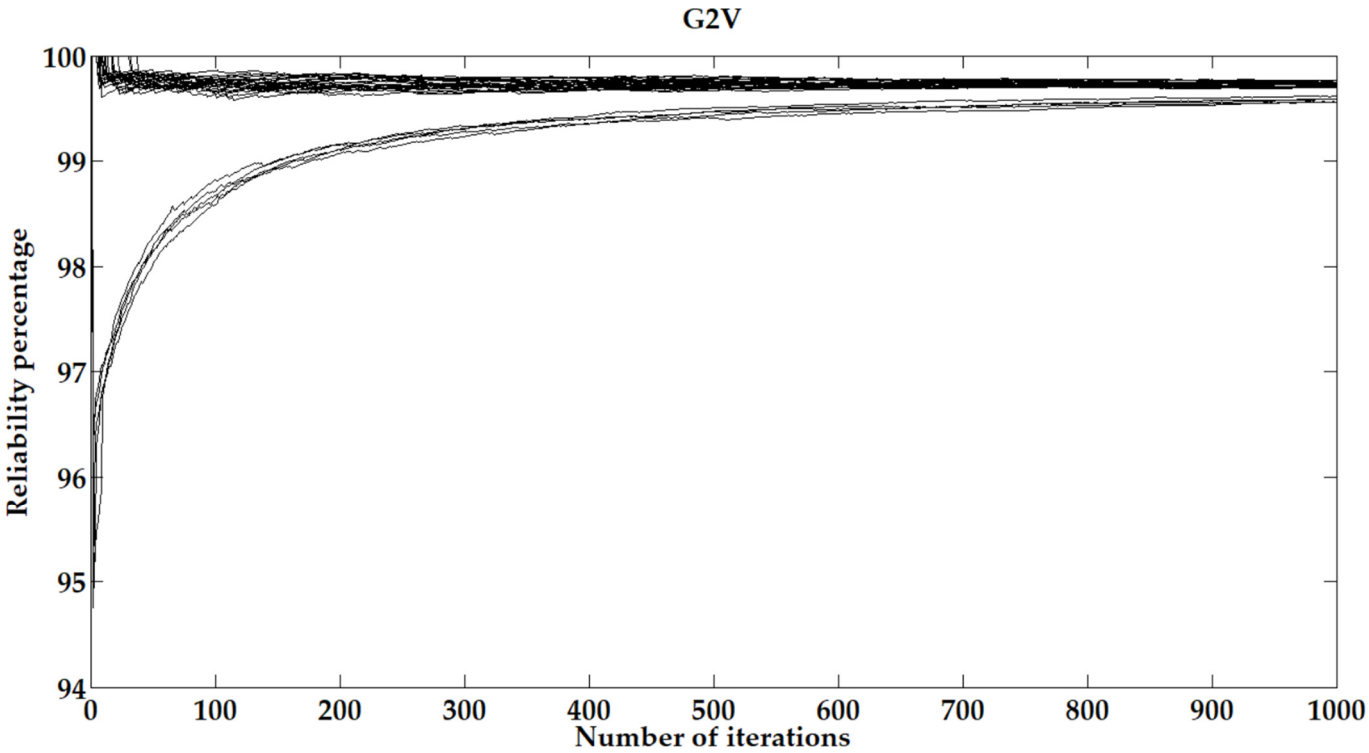

Figure 6. Plot of grid reliability percentage in G2V for two EVs.

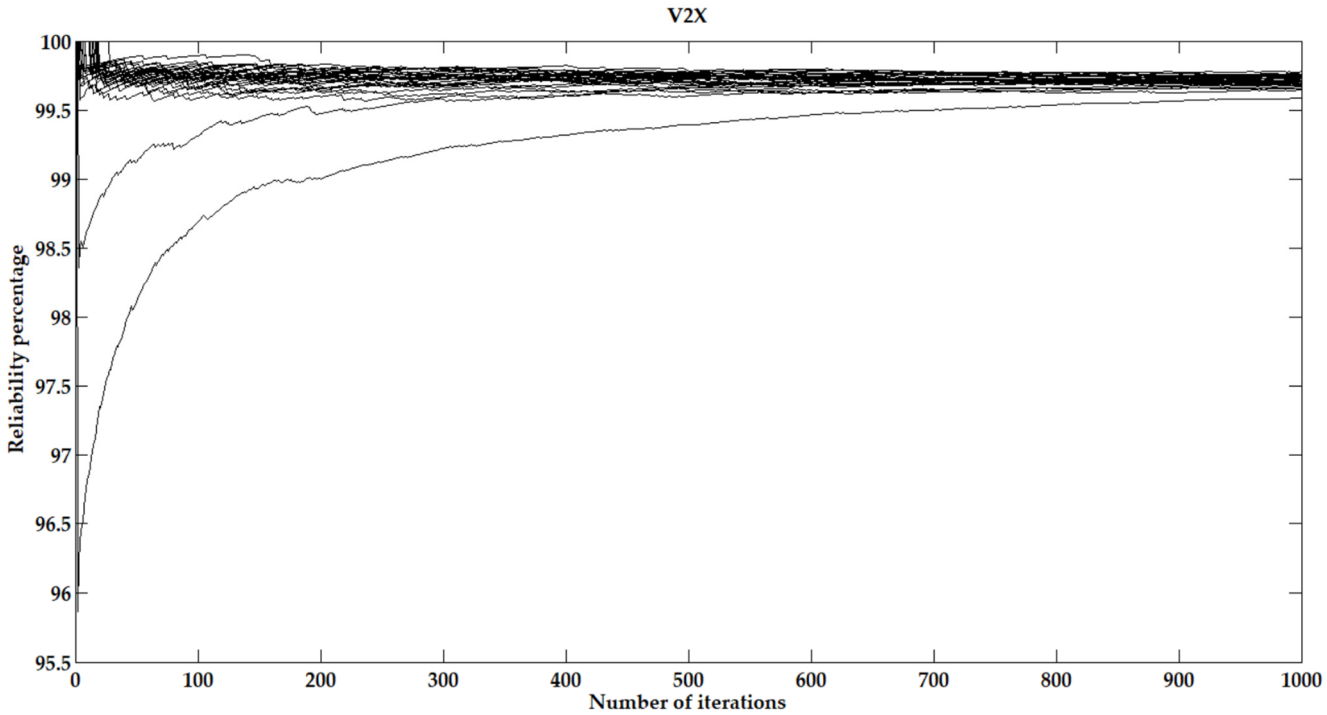

Figure 7. Plot of grid reliability percentage in V2X for two EVs.

https://doi.org/10.3390/wevj17120635

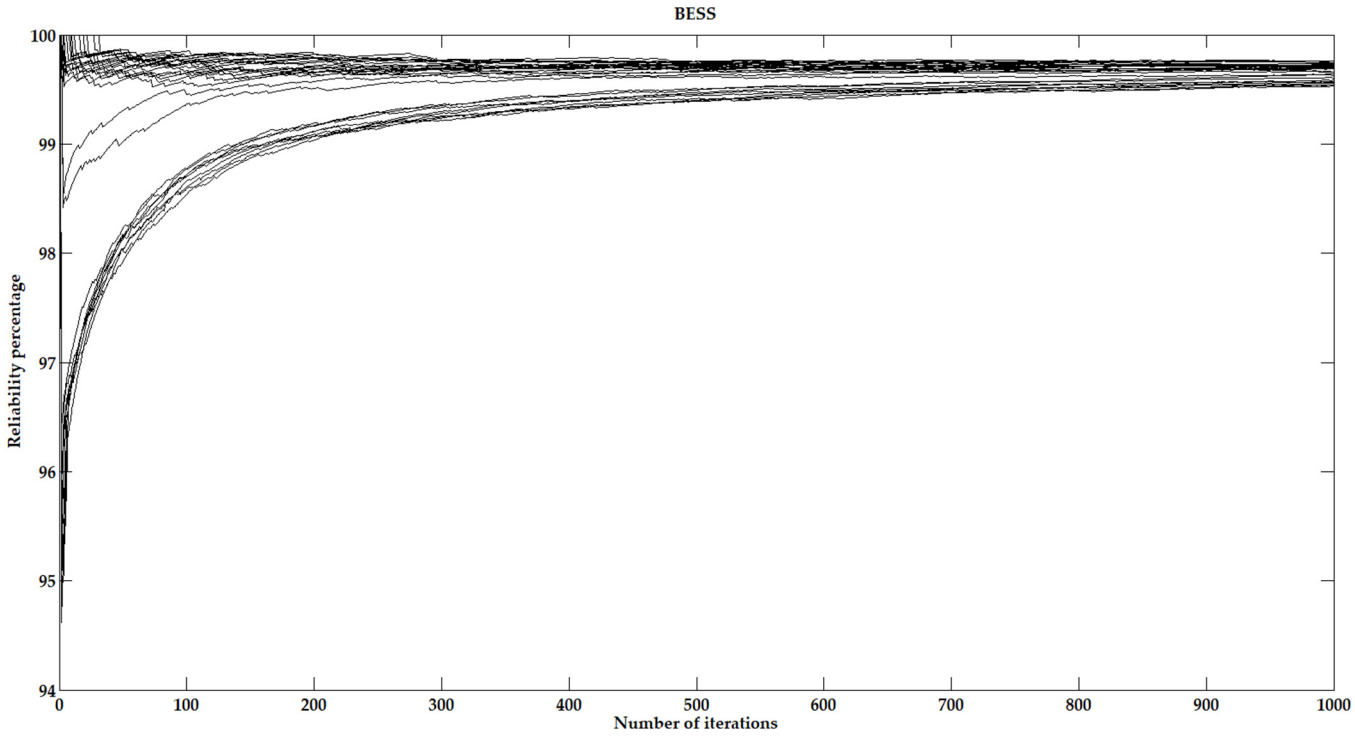

Figure 8. Plot of grid reliability percentage in stationary BESS for two EVs.

Table 3. Reliability percentages for thirty runs for G2V, V2X and BESS cases for two EVs.

	Reliability (%)		
Seed Count	**G2V (%)**	**V2X (%)**	**BESS (%)**
1	99.7060	99.7374	99.6046
2	99.6137	99.5861	99.7116
3	99.5582	99.7566	99.6925
4	99.7152	99.6754	99.7128
5	99.7384	99.6664	99.7125
6	99.7313	99.643	99.6945
7	99.7465	99.6937	99.7577
8	99.5887	99.7103	99.6917
9	99.7019	99.6924	99.7598
10	99.7494	99.7049	99.7136
11	99.7076	99.7277	99.6995
12	99.555	99.7116	99.6872
13	99.7018	99.7306	99.7574
14	99.7058	99.7552	99.7116
15	99.7309	99.7514	99.7588
16	99.5892	99.7434	99.6309
17	99.7686	99.724	99.7204
18	99.7326	99.7413	99.7594
19	99.7469	99.6926	99.734
20	99.7421	99.6785	99.7043
21	99.7691	99.6942	99.7421
22	99.7484	99.7763	99.6623
23	99.7316	99.6927	99.6407
24	99.6992	99.7070	99.7297
25	99.6945	99.7053	99.6564

26	99.7334	99.7347	99.7429
27	99.7385	99.7283	99.7611
28	99.7456	99.6514	99.7475
29	99.7443	99.7264	99.691
30	99.7623	99.6938	99.7598
Mean	99.7066	99.7078	99.7116
SD	0.06123	0.03908	0.04181
Confidence Interval 95%	[99.6837, 99.7294]	[99.6932, 99.7223]	[99.696, 99.7272]

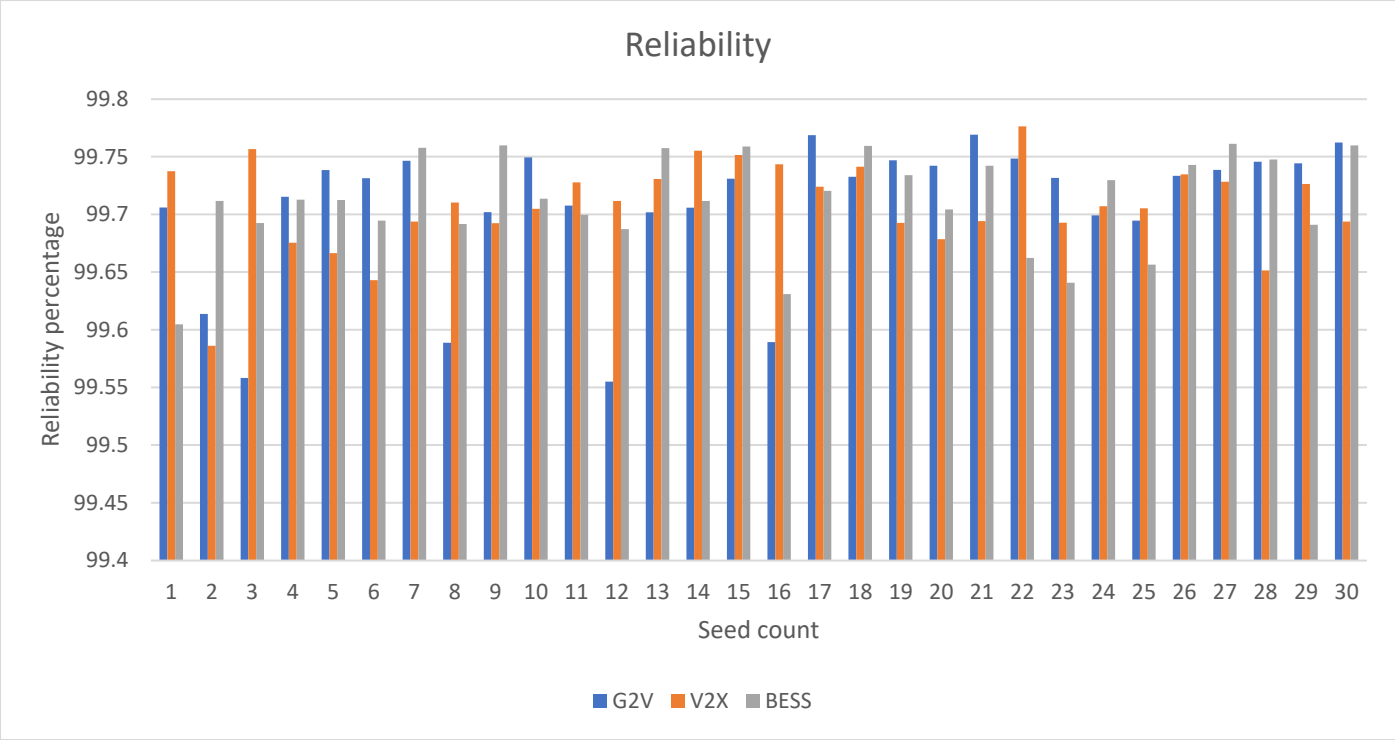

Figure 9. Line plot of reliability percentages for thirty runs for G2V, V2X and BESS cases for two EVs.

A summary of grid reliability in all three cases with two EVs is shown in Table 4. Grid reliability is jittery throughout the simulation because of natural variations due to VRE. Demand–supply balance is achieved in the microgrid despite the presence of VRE as a source and randomly occurring demand spikes in terms of quantity of energy and timing.

Table 4. Summary of reliability of electric energy supply in G2V, V2X and BESS for two EVs.

Grid Reliability	G2V	V2X	Stationary BESS
Mean	99.7066%	99.7078%	99.7116%
Standard deviation	0.06123%	0.03908%	0.04181%

3.2. VRE Curtailment with Two EVs

VRE Curtailment for G2V, V2X and stationary BESS is simulated thirty times with two EVs. Each time, a different seed but with the same sequence is chosen.

Graphical results for curtailment in the case of G2V are shown in Figure 10. Graphical results for curtailment in the case of V2X are shown in Figure 11. Graphical results for

curtailment in the case of BESS are shown in Figure 12. Figure 13 shows line plots of VRE curtailments in all three cases.

Table 5 tabulates the results of thirty runs for curtailment in all three cases.

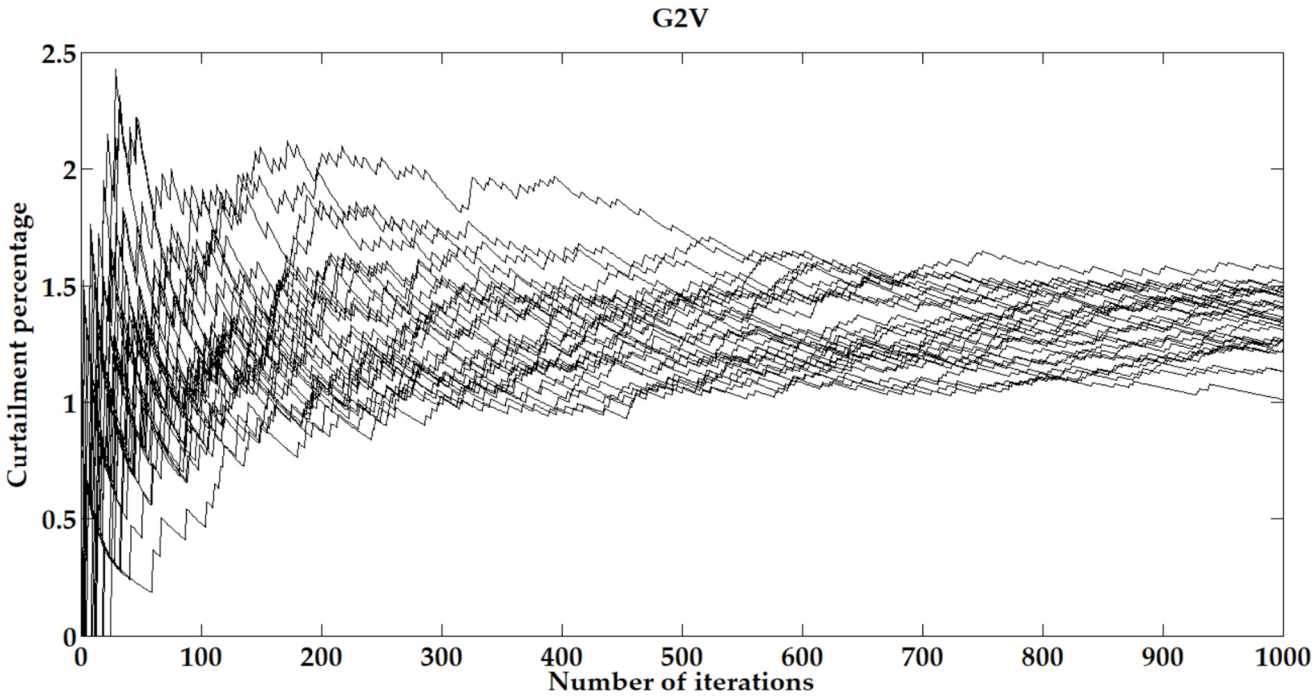

Figure 10. Plot of curtailment percentage in G2V with two EVs.

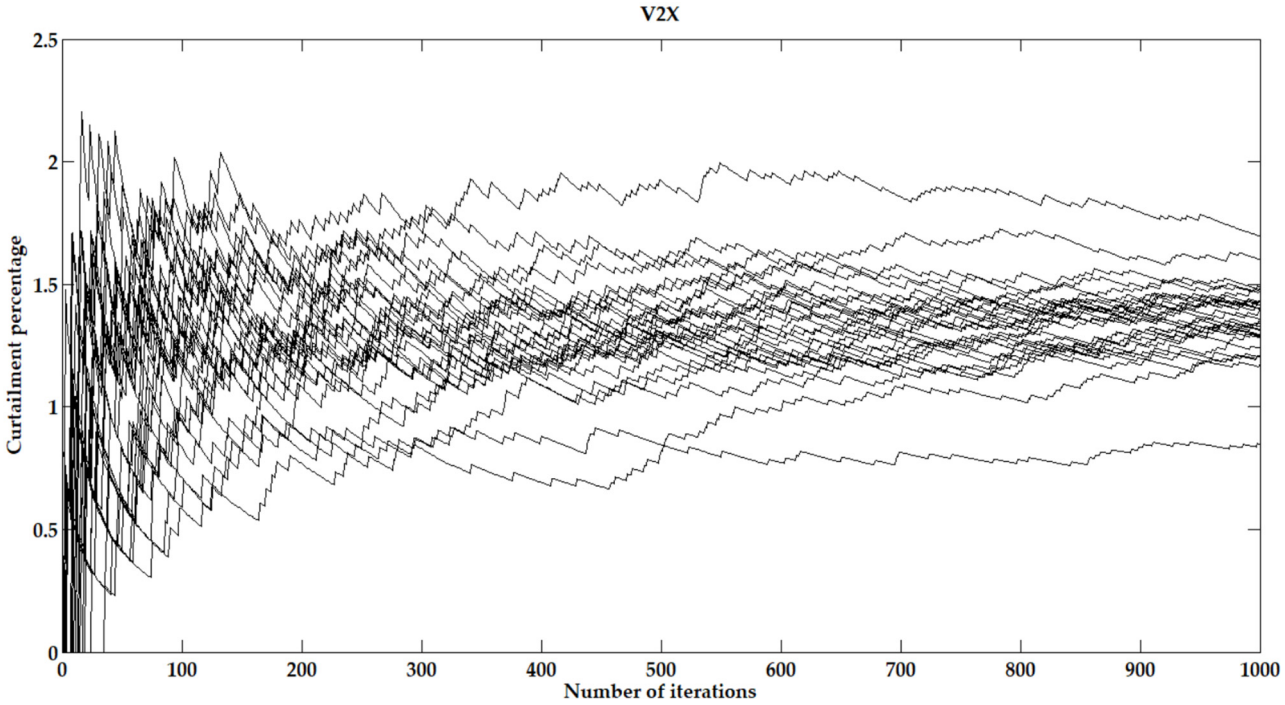

Figure 11. Plot of curtailment percentage in V2X with two EVs.

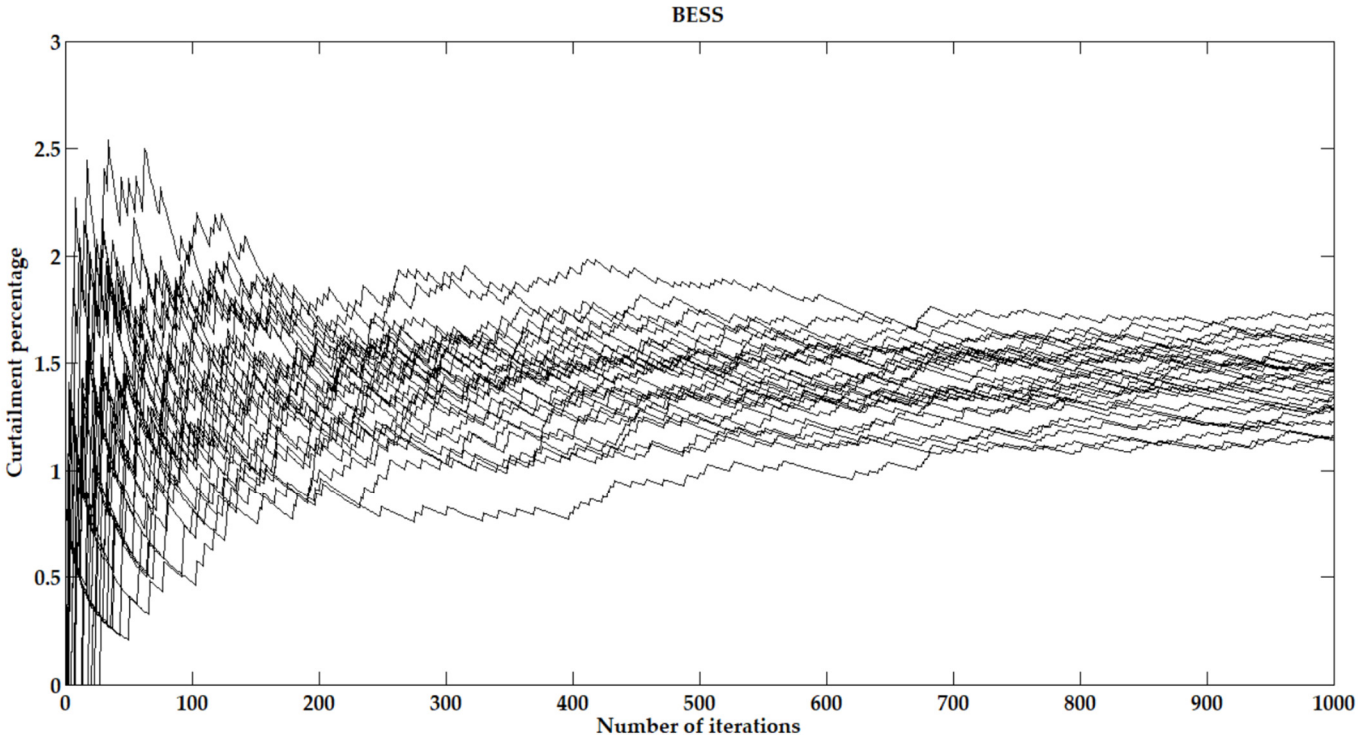

Figure 12. Plot of curtailment percentage in BESS with two EVs.

Table 5. Curtailment percentages for thirty runs for G2V, V2X and BESS cases with two EVs.

	Curtailment (%)		
Seed Count	**G2V (%)**	**V2X (%)**	**BESS (%)**
1	1.3629	1.358	1.325
2	1.3367	1.2032	1.4504
3	1.4656	1.4759	1.4802
4	1.4684	1.402	1.2647
5	1.7245	1.3121	1.2599
6	1.5285	1.2014	1.4056
7	1.292	1.4914	1.4909
8	1.5906	1.2942	1.3389
9	1.4595	1.6016	1.2705
10	1.2242	1.1758	1.1333
11	1.2869	1.4866	1.2687
12	1.4804	1.2893	1.3122
13	1.1398	1.3408	1.3987
14	1.3114	1.3266	1.4269
15	1.4176	1.2863	1.4097
16	1.2805	1.2056	1.4705
17	1.502	1.4135	1.2138
18	1.6233	1.4264	1.4842
19	1.3442	1.2825	1.3595
20	1.2256	1.4349	1.4569
21	1.6125	1.3499	1.1338
22	1.1599	1.2387	1.3524
23	1.3614	0.8485	1.2136
24	1.4593	1.4294	1.5135
25	1.4959	1.4783	1.2633

26	1.4122	1.4269	1.3657
27	1.4321	1.3989	1.2282
28	1.6746	1.3979	1.5695
29	1.1514	1.3157	1.0135
30	1.5644	1.6949	1.3414
Mean	1.4129	1.3529	1.3405
SD	0.1553	0.1517	0.128
Confidence Interval 95%	[0.1237, 0.2087]	[0.1208, 0.2039]	[0.102, 0.1721]

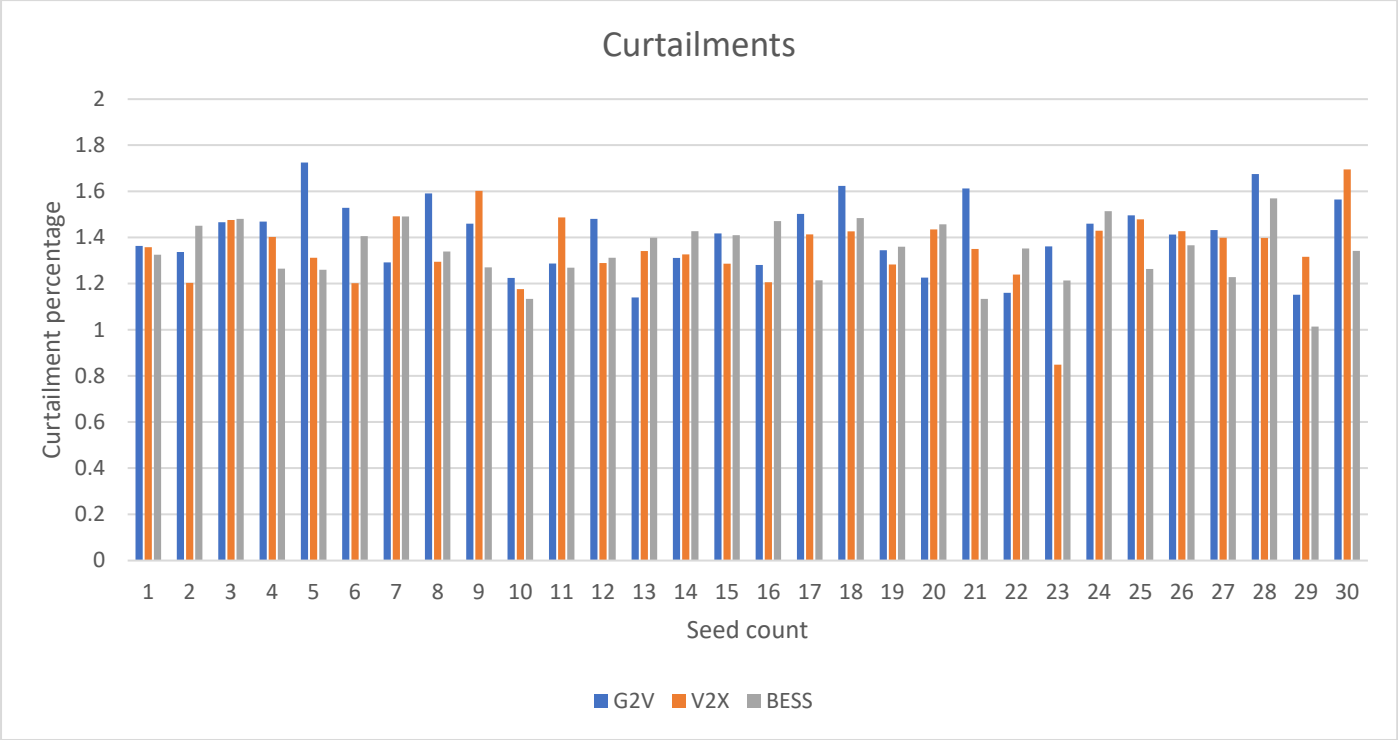

Figure 13. Line plot of curtailment percentages for thirty runs for G2V, V2X and BESS cases with two EVs.

Summary of curtailment in all three cases is shown in Table 6. Grid curtailment fluctuates throughout the simulation due to natural variations from VRE. Demand-supply balance is achieved in the microgrid despite the presence of VRE as a source and randomly occurring demand spikes in terms of quantity of energy and timing.

Table 6. Summary of curtailment of electric energy supply in G2V, V2X and BESS with two EVs.

Grid Curtailment	G2V	V2X	Stationary BESS
Mean	1.4129%	1.3529%	1.3405%
Standard deviation	0.1280%	0.1517%	0.1553%

3.3. Non-Dispatchability with Two EVs

Non-dispatchability for G2V, V2X and stationary BESS is simulated thirty times with two EVs. Each time, a different seed but with the same sequence is chosen for all three cases.

Graphical results for non-dispatchability in the case of G2V are shown in Figure 14. Graphical results for non-dispatchability in the case of V2X are shown in Figure 15. Graphical results for non-dispatchability in the case of BESS are shown in Figure 16.

Table 7 tabulates non-dispatchability percentages for thirty runs for G2V, V2X and BESS cases.

Figure 17 shows non-dispatchability in all three cases in the form of a line plot.

Summary of results of thirty runs for non-dispatchability in all three cases is tabulated in Table 8.

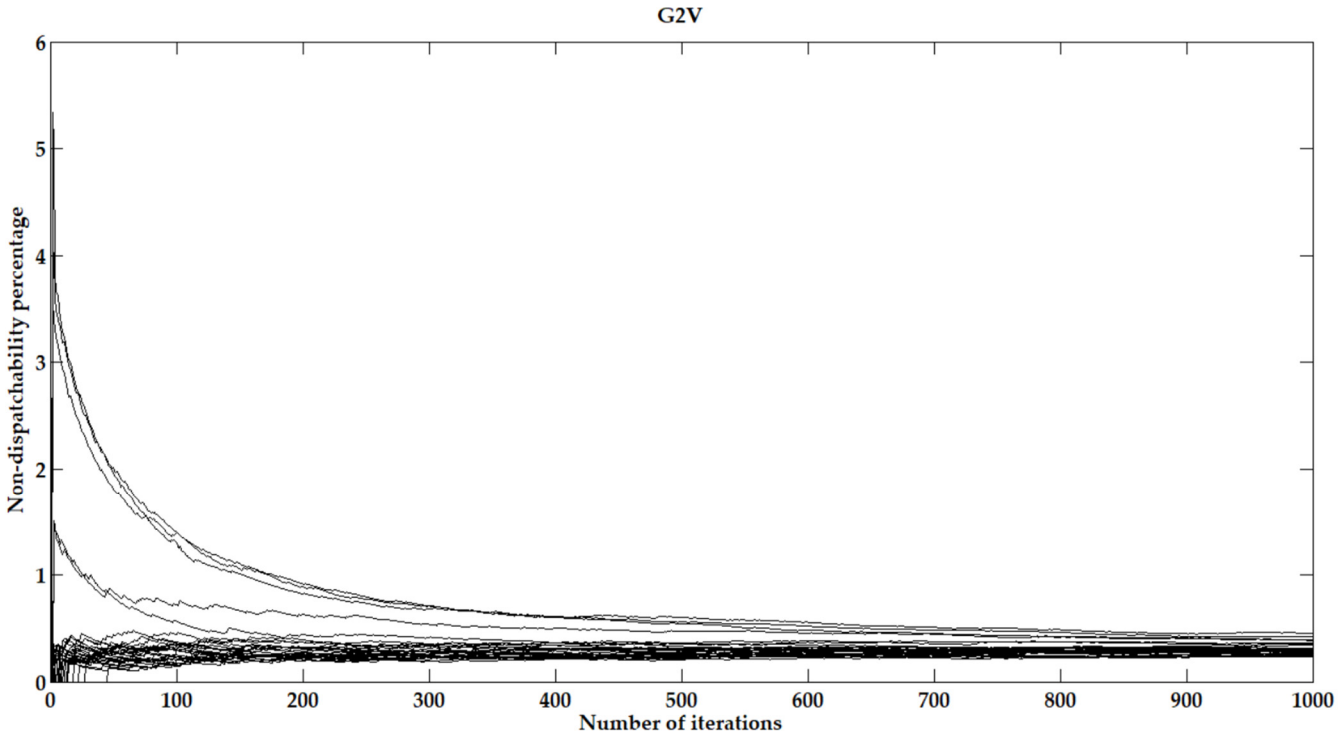

Figure 14. Plot of non-dispatchability percentage in G2V with two EVs.

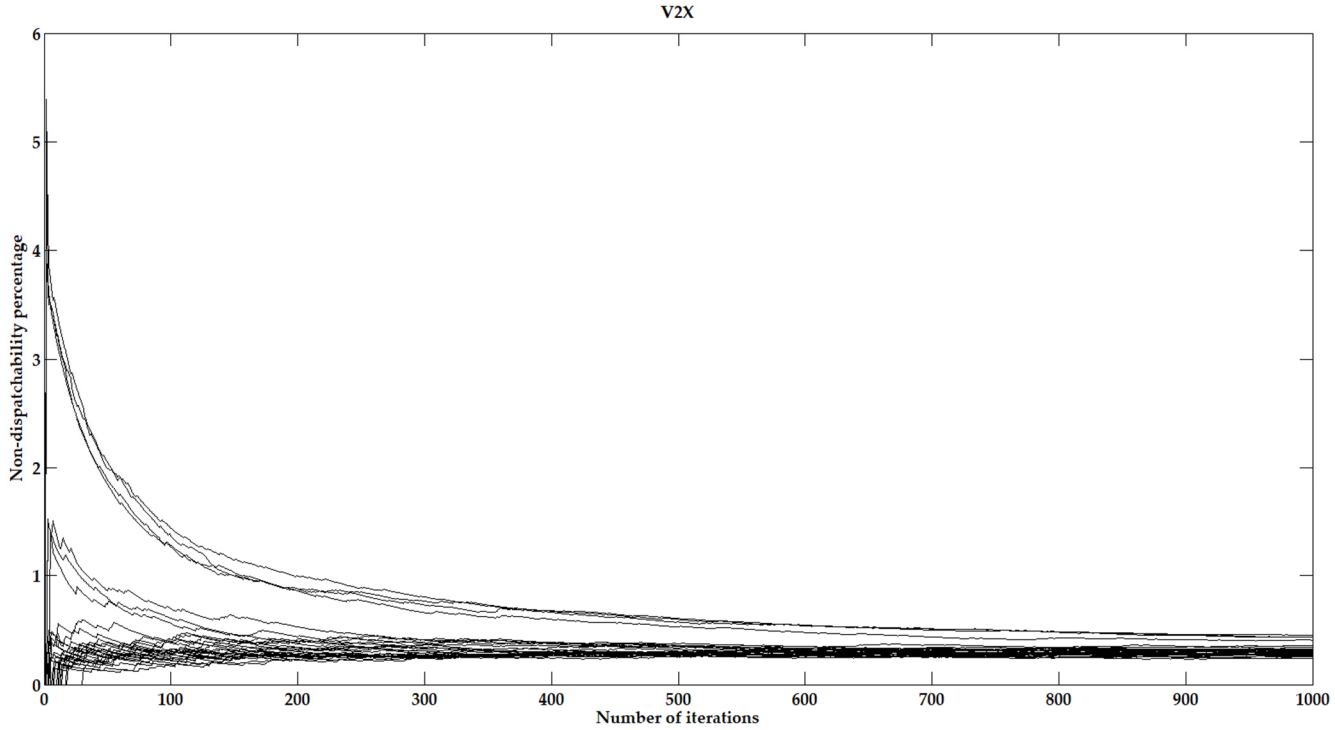

Figure 15. Plot of non-dispatchability percentage in V2X with two EVs.

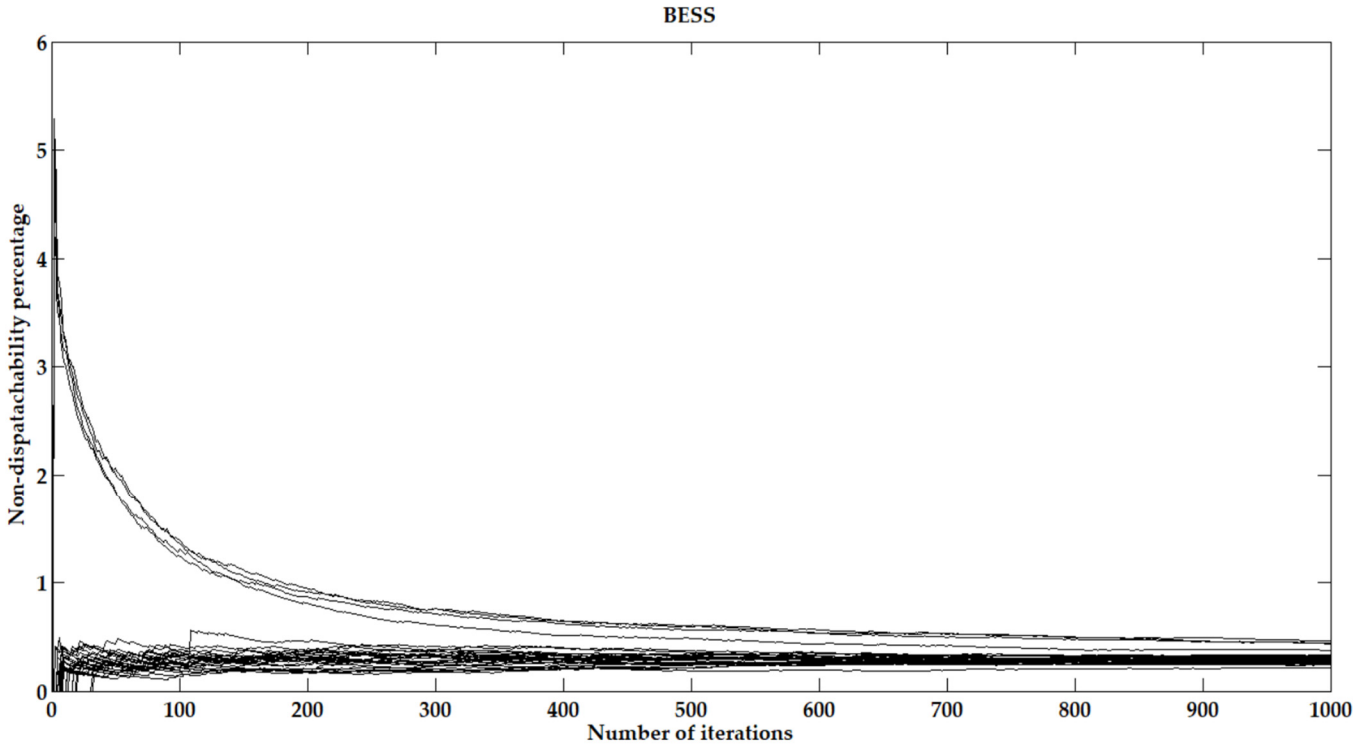

Figure 16. Plot of non-dispatchability percentage in BESS with two EVs.

Table 7. Non-dispatchability percentages for thirty runs for G2V, V2X and BESS cases with two EVs.

	Non-Dispatchability (%)		
Seed Count	**G2V (%)**	**V2X (%)**	**BESS (%)**
1	0.2795	0.2724	0.2683
2	0.2892	0.3497	0.4358
3	0.2976	0.3132	0.3027
4	0.3534	0.2839	0.2579
5	0.4341	0.426	0.2698
6	0.3377	0.2342	0.2985
7	0.2762	0.2949	0.2404
8	0.3186	0.2966	0.2868
9	0.325	0.2448	0.33
10	0.3195	0.3028	0.4439
11	0.4077	0.2523	0.2963
12	0.2719	0.271	0.2776
13	0.3262	0.2859	0.3238
14	0.448	0.2865	0.3053
15	0.3045	0.2869	0.2813
16	0.2903	0.3393	0.2742
17	0.2691	0.3608	0.2501
18	0.4329	0.295	0.2905
19	0.2984	0.386	0.2976
20	0.3102	0.2755	0.2482
21	0.3197	0.3919	0.3137
22	0.2585	0.2488	0.4587
23	0.3047	0.2946	0.3755
24	0.3026	0.2659	0.2638
25	0.2385	0.2876	0.2597

26	0.2596	0.3025	0.2704
27	0.2414	0.3012	0.3018
28	0.2892	0.3068	0.3263
29	0.2697	0.4571	0.2164
30	0.2892	0.2488	0.298
Mean	0.3121	0.3054	0.3021
SD	0.05454	0.05343	0.05793
Confidence Interval 95%	[0.04344, 0.07332]	[0.04255, 0.07182]	[0.04613, 0.07787]

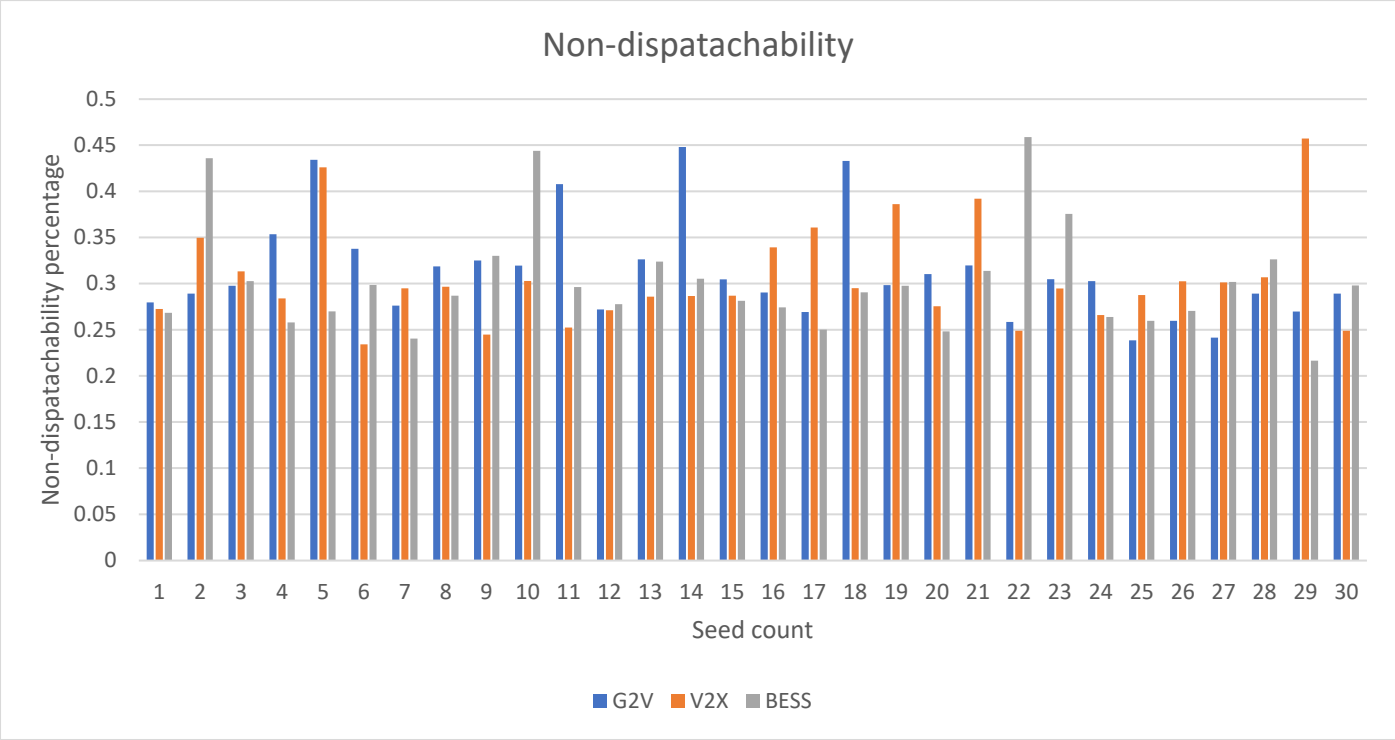

Figure 17. Line plot of non-dispatchability percentages for thirty runs for G2V, V2X and BESS cases with two EVs.

Table 8. Summary of non-dispatchability of electric energy supply in G2V, V2X and BESS with two EVs.

Grid Non-Dispatchability	G2V	V2X	Stationary BESS
Mean	0.3121%	0.3054%	0.3021%
Standard deviation	0.05343%	0.05454%	0.05793%

3.4. Grid Reliability with One EV

Grid reliability for G2V, V2X, and stationary BESS is simulated thirty times for one EV. Each time, a different seed but with the same sequence is chosen for all three cases.

Graphical results for reliability in the case of G2V are shown in Figure 18. Graphical results for reliability in the case of V2X are shown in Figure 19. Graphical results for reliability in the case of stationary BESS are shown in Figure 20. Figure 21 plots the three cases with a single EV together.

Results of thirty runs for reliability in all three cases are tabulated in Table 9.

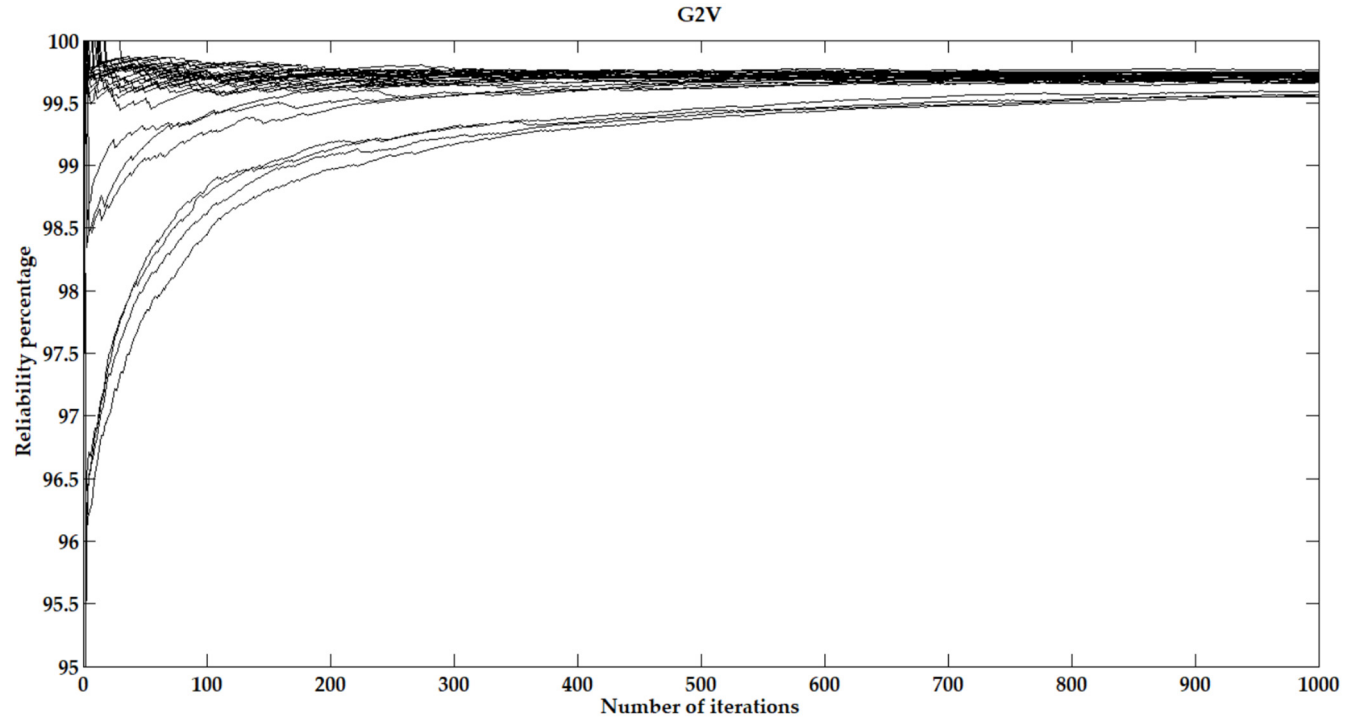

Figure 18. Plot of grid reliability percentage in G2V for one EV.

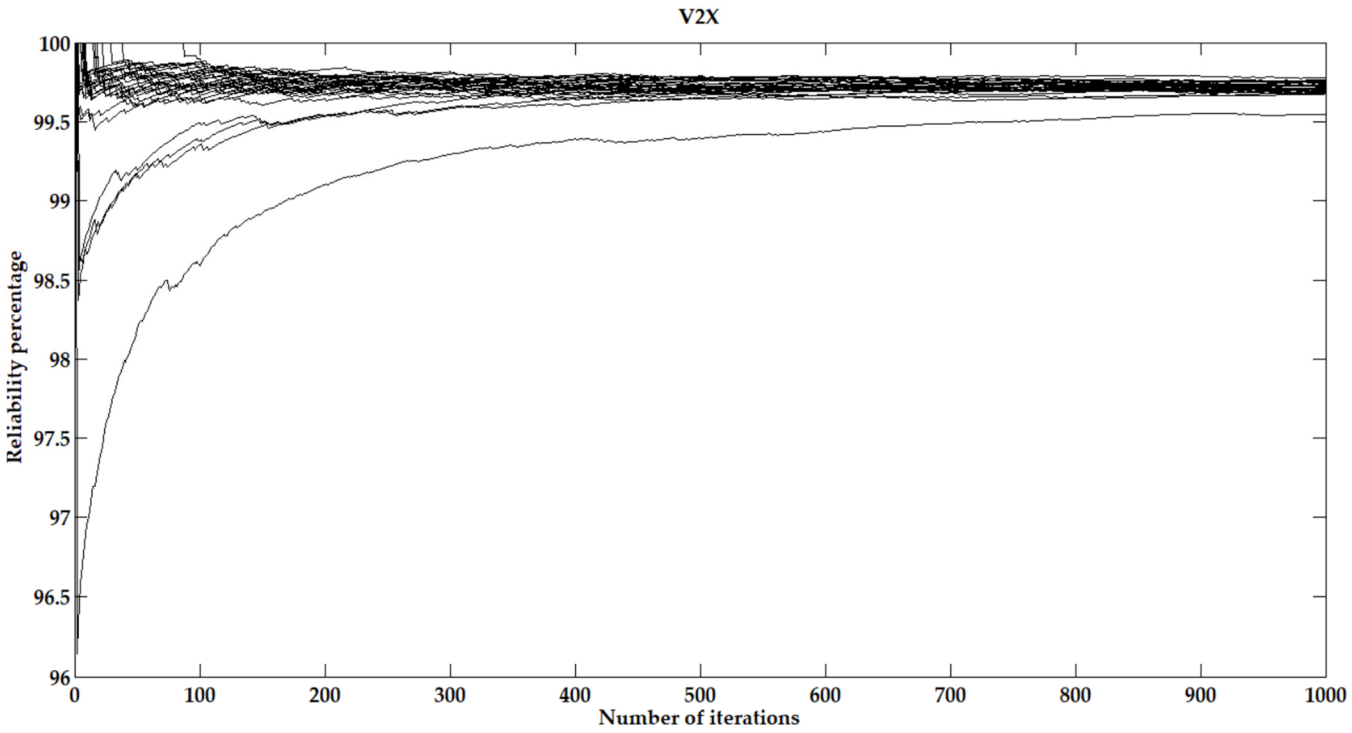

Figure 19. Plot of grid reliability percentage in V2X for one EV.

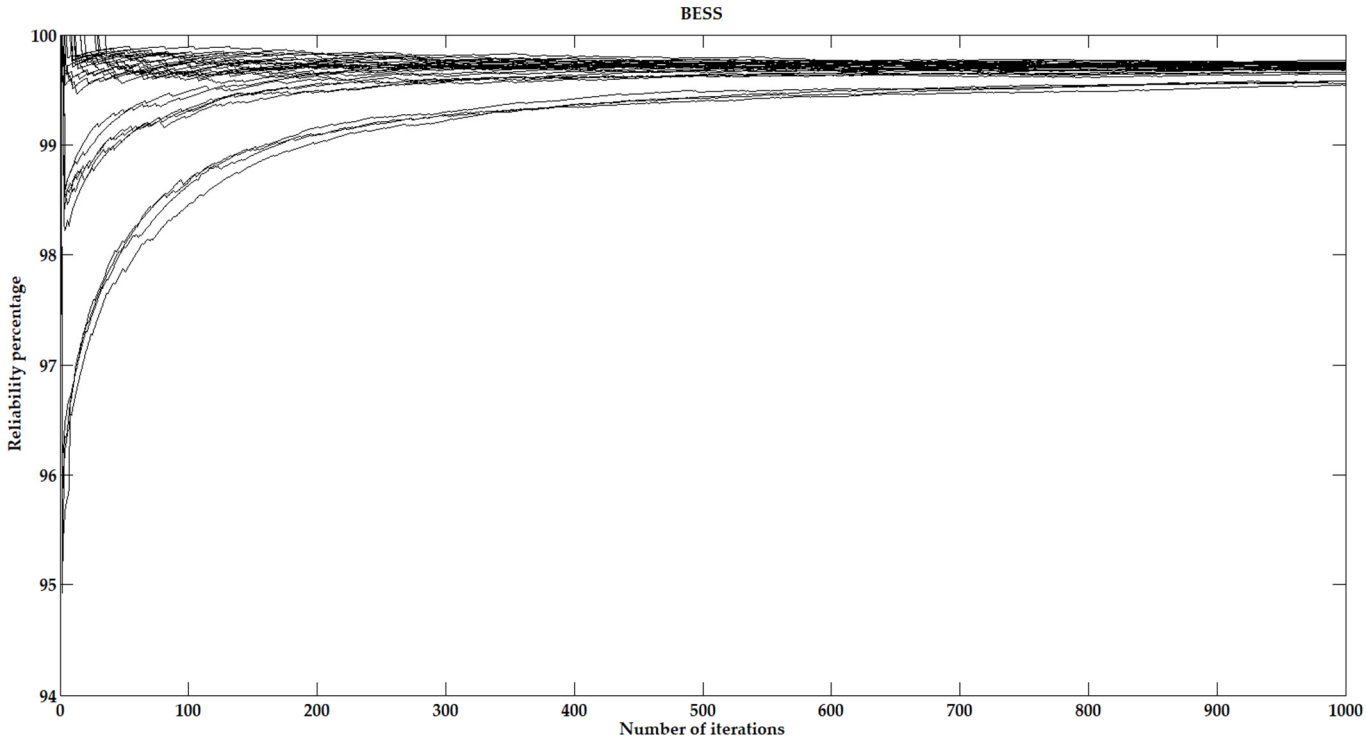

Figure 20. Plot of grid reliability percentage in stationary BESS for one EV.

Table 9. Reliability percentages for thirty runs for G2V, V2X and BESS cases for one EV.

	Reliability (%)		
Seed Count	**G2V (%)**	**V2X (%)**	**BESS (%)**
1	99.6862	99.724	99.7333
2	99.7227	99.7266	99.6968
3	99.7165	99.6608	99.6911
4	99.692	99.5663	99.7112
5	99.7448	99.6682	99.545
6	99.7426	99.7406	99.7545
7	99.6853	99.7067	99.7648
8	99.7381	99.6821	99.7472
9	99.6423	99.7263	99.6784
10	99.737	99.5888	99.705
11	99.6878	99.7306	99.6897
12	99.5812	99.6731	99.7269
13	99.7425	99.5616	99.6964
14	99.7497	99.6901	99.7319
15	99.7301	99.7137	99.7539
16	99.7152	99.7191	99.6835
17	99.6993	99.5521	99.7503
18	99.6969	99.7001	99.7279
19	99.7088	99.6873	99.6752
20	99.7373	99.704	99.7174
21	99.6591	99.739	99.6857
22	99.7702	99.7045	99.6931
23	99.5429	99.7001	99.7325
24	99.5809	99.7619	99.7282
25	99.7222	99.7337	99.7295

26	99.5593	99.7479	99.7104
27	99.6609	99.7204	99.7455
28	99.7394	99.7407	99.6838
29	99.7348	99.7077	99.7359
30	99.6782	99.7338	99.7784
Mean	99.6935	99.6937	99.7134
SD	0.0592	0.05608	0.04232
Confidence Interval 95%	[99.6714, 99.7156]	[99.6728, 99.7147]	[99.6976, 99.7292]

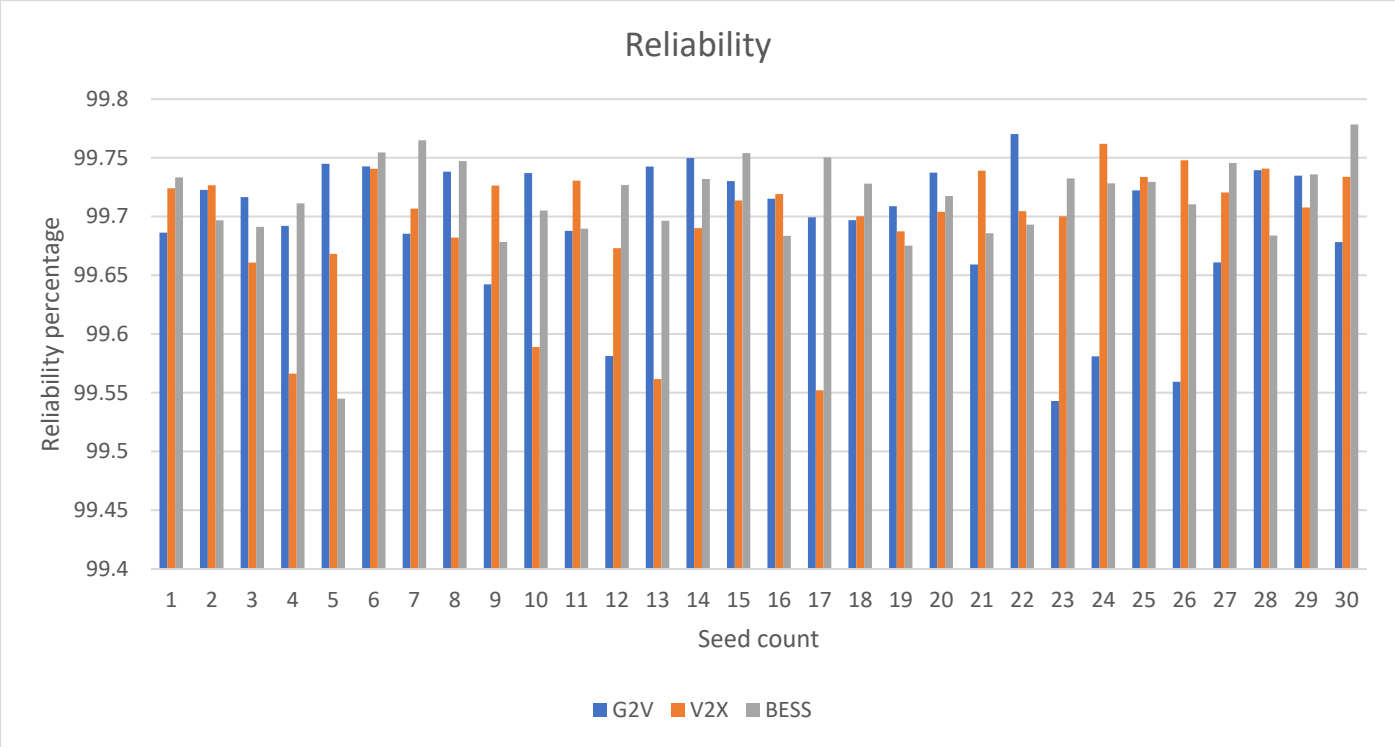

Figure 21. Line plot of reliability percentages for thirty runs for G2V, V2X and BESS cases for one EV.

Summary of grid reliability in all three cases is shown in Table 10. Grid reliability is jittery throughout the simulation because of natural variations due to VRE. Demand–supply balance is achieved in the microgrid despite the presence of VRE as a source and randomly occurring demand spikes in terms of quantity of energy and timing.

Table 10. Summary of reliability of electric energy supply in G2V, V2X and BESS for one EV.

Grid Reliability	G2V	V2X	Stationary BESS
Mean	99.6935%	99.6937%	99.7134%
Standard deviation	0.0592%	0.05608%	0.04232%

3.5. VRE Curtailment with One EV

VRE curtailment for G2V, V2X and stationary BESS is simulated thirty times with one EV. Each time, a different seed but with the same sequence is chosen for all three cases.

Graphical results for curtailment in the case of G2V are shown in Figure 22. Graphical results for curtailment in the case of V2X are shown in Figure 23. Graphical results for

curtailment in the case of BESS are shown in Figure 24. Figure 25 shows line plots of VRE curtailments in all three cases.

Results of thirty runs for curtailment in all three cases are tabulated in Table 11.

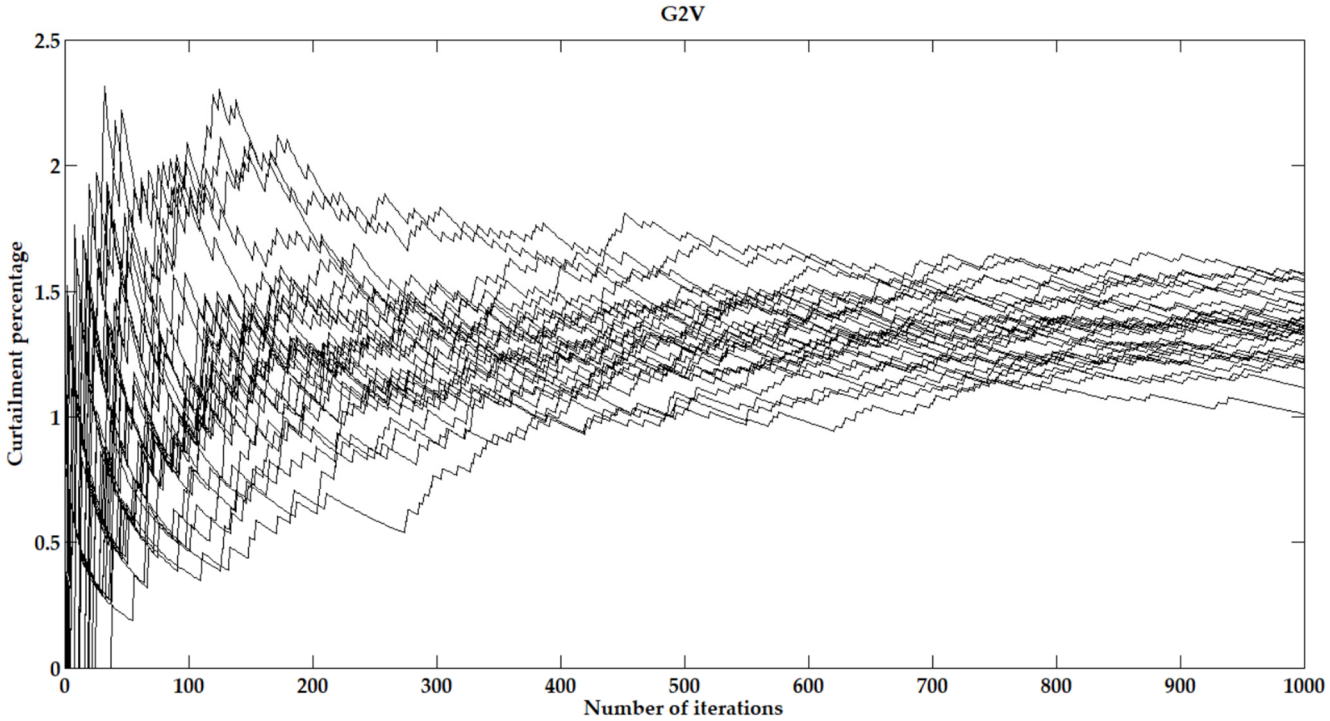

Figure 22. Plot of curtailment percentage in G2V with one EV.

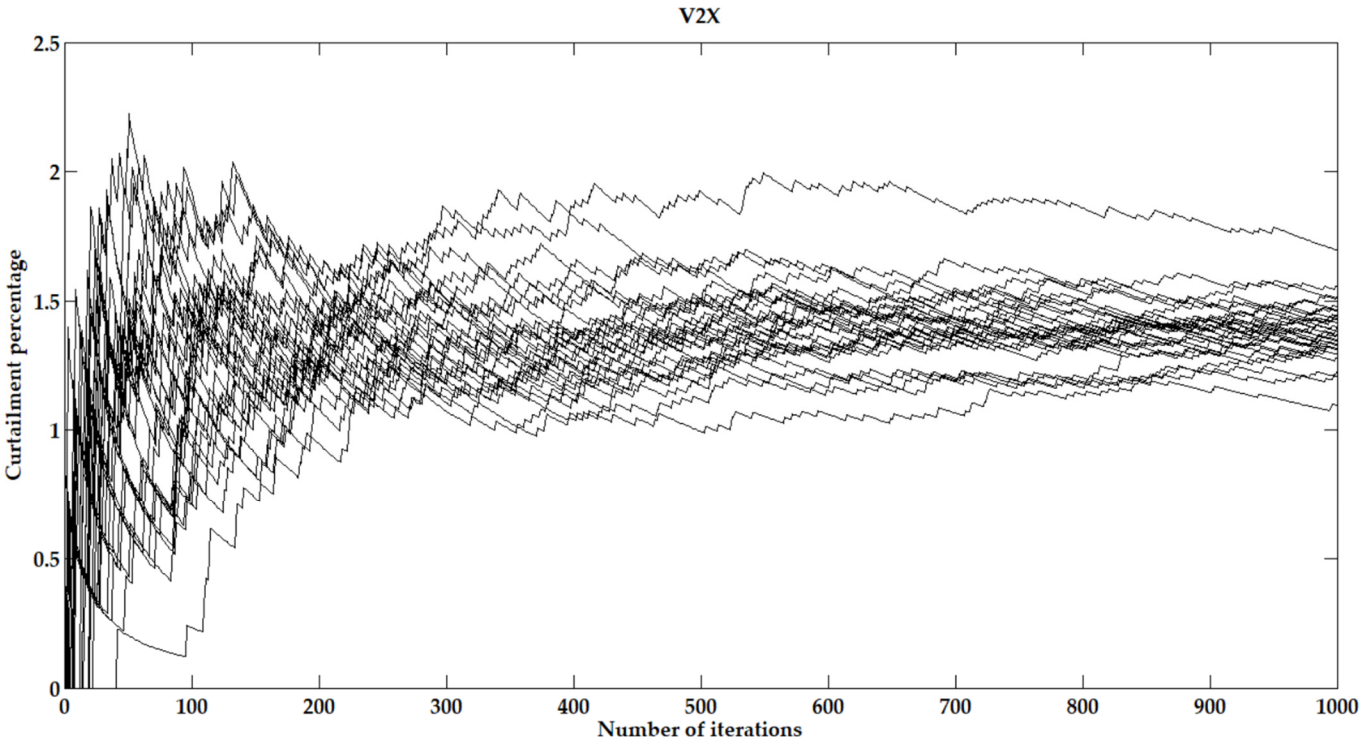

Figure 23. Plot of curtailment percentage in V2X with one EV.

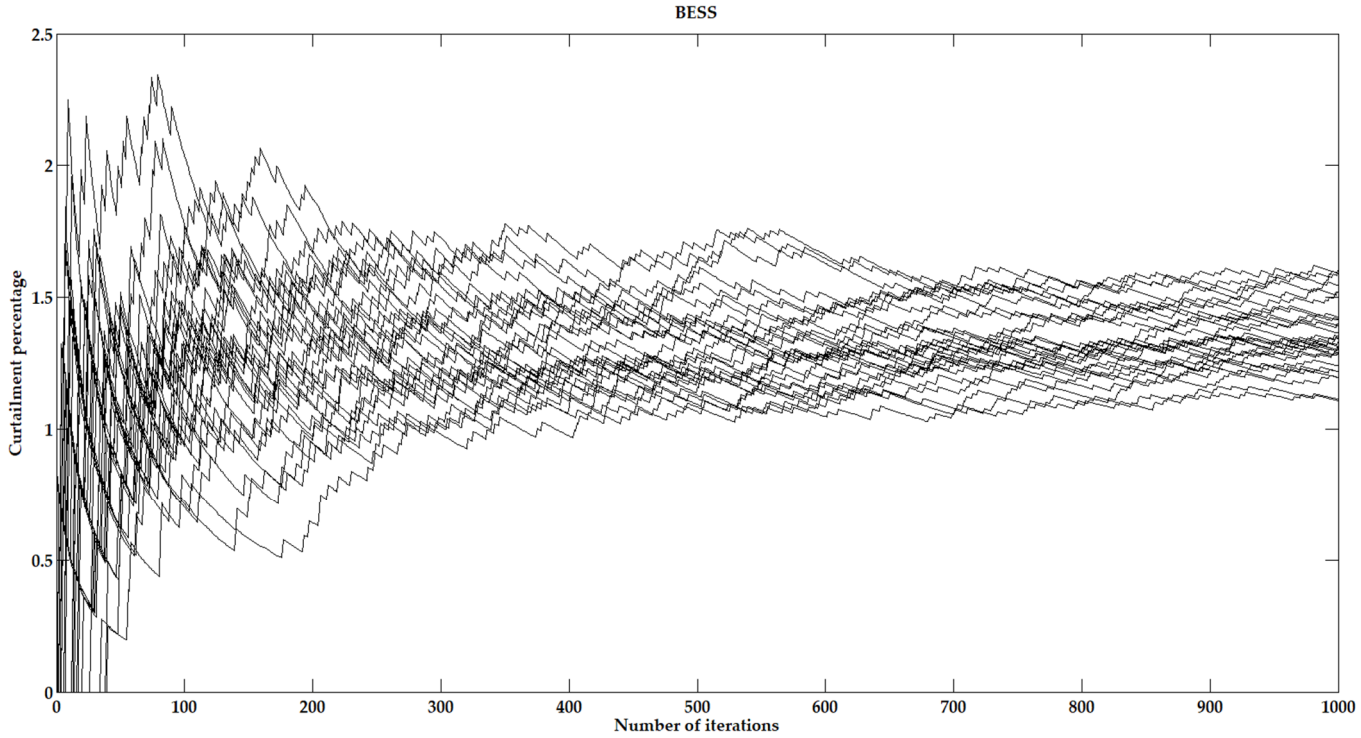

Figure 24. Plot of curtailment percentage in BESS with one EV.

Table 11. Curtailment percentages for thirty runs for G2V, V2X and BESS cases with one EV.

	Curtailment (%)		
Seed Count	**G2V (%)**	**V2X (%)**	**BESS (%)**
1	1.4783	1.5905	1.3657
2	1.4269	1.6037	1.2282
3	1.3989	1.2181	1.5695
4	1.3979	1.3432	1.0135
5	1.3157	1.425	1.3414
6	1.6949	1.1962	1.1175
7	1.2936	1.3323	1.2169
8	1.4629	1.3002	1.3137
9	1.5113	1.3964	1.1914
10	1.3283	1.3923	1.4561
11	1.4417	1.1133	1.4254
12	1.4599	1.5171	1.5459
13	1.349	1.3463	1.3538
14	1.3649	1.2401	1.2304
15	1.44	1.2922	1.3438
16	1.4326	1.5444	1.5374
17	1.3443	1.2838	1.3599
18	1.0971	1.3095	1.2967
19	1.5542	1.2892	1.3549
20	1.4149	1.4126	1.3789
21	1.3167	1.1079	1.2411
22	1.5184	1.5187	1.4446
23	1.2069	1.3074	1.2332
24	1.2787	1.3508	1.3259
25	1.2928	1.3633	1.3899

26	1.3828	1.3139	1.565
27	1.3741	1.2173	1.4759
28	1.3108	1.4177	1.3464
29	1.2291	1.1949	1.3605
30	1.3331	1.5939	1.394
Mean	1.3817	1.3511	1.3473
SD	0.1147	0.1342	0.1292
Confidence Interval 95%	[1.3389, 1.4245]	[1.3009, 1.4012]	[1.299, 1.3955]

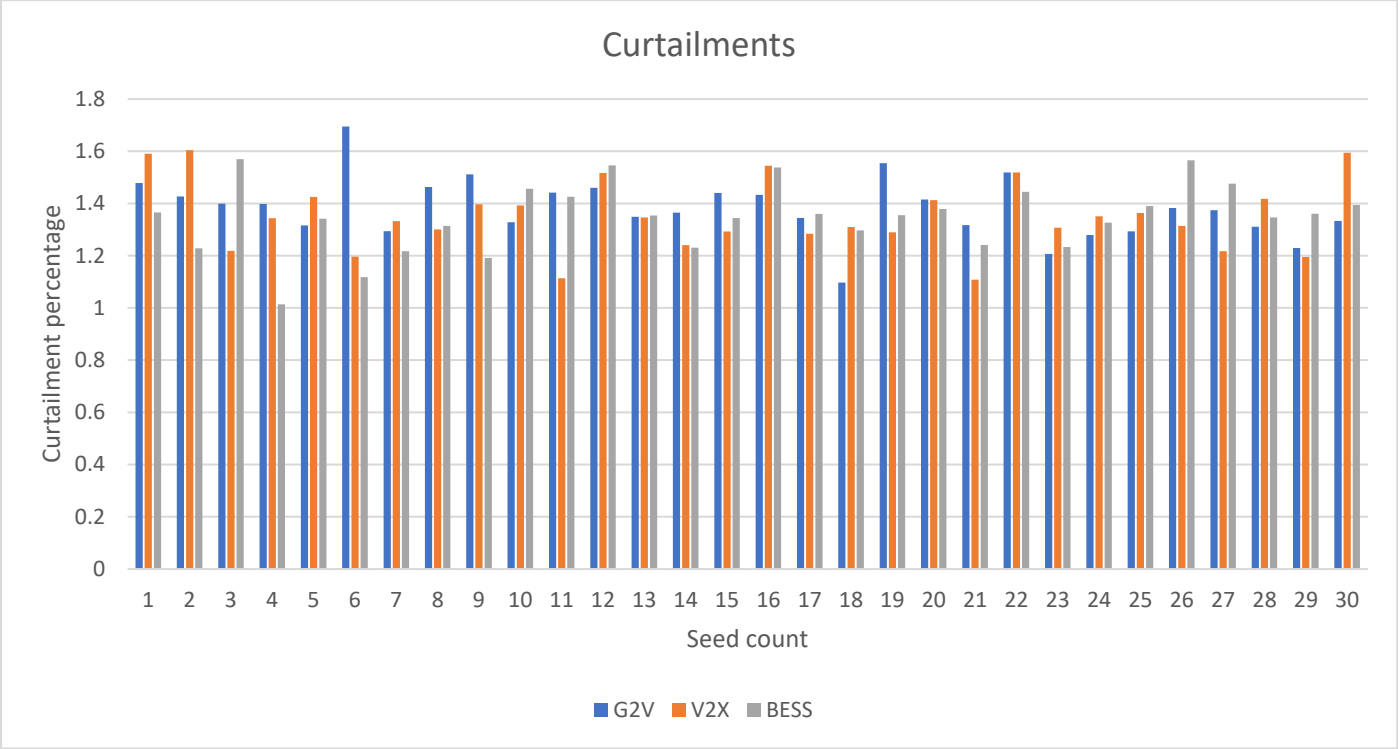

Figure 25. Line plot of curtailment percentages for thirty runs for G2V, V2X and BESS cases with one EV.

Summary of curtailment in all three cases is shown in Table 12. Grid curtailment is jittery throughout the simulation because of natural variations due to VRE. Demand–supply balance is achieved in the microgrid despite the presence of VRE as a source and randomly occurring demand spikes in terms of quantity of energy and timing.

Table 12. Summary of curtailment of electric energy supply in G2V, V2X and BESS with one EV.

Grid Curtailment	G2V	V2X	Stationary BESS
Mean	1.3817%	1.3511%	1.3473%
Standard deviation	0.1147%	0.1342%	0.1292%

3.6. Non-Dispatchability with One EV

Non-dispatchability for G2V, V2X and stationary BESS is simulated thirty times with one EV. Each time, a different seed but with the same sequence is chosen for all three cases.

Graphical results for non-dispatchability in the case of G2V are shown in Figure 26. Graphical results for non-dispatchability in the case of V2X are shown in Figure 27. Graphical results for non-dispatchability in the case of BESS are shown in Figure 28.

Table 13 tabulates non-dispatchability percentages for thirty runs for G2V, V2X and BESS cases.

Figure 29 shows non-dispatchability in all three cases in the form of a line plot.

Summary of results of thirty runs for non-dispatchability in all three cases is tabulated in Table 14.

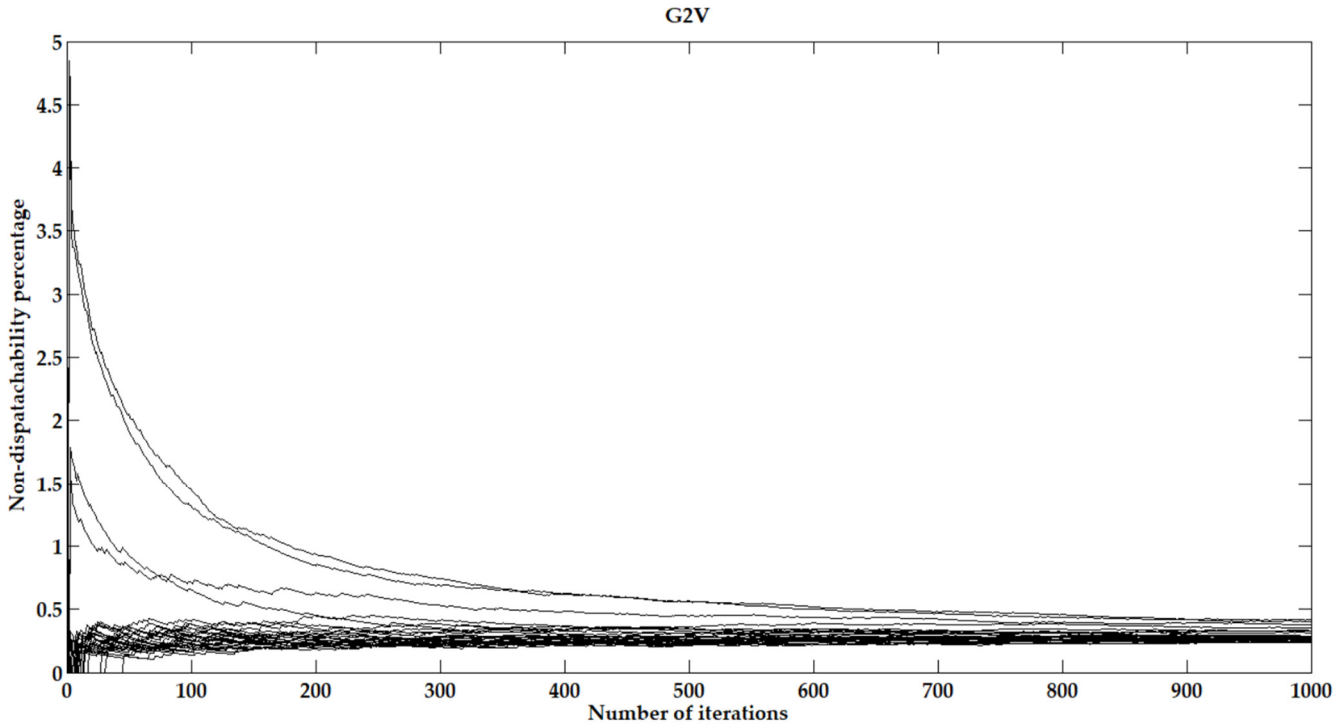

Figure 26. Plot of non-dispatchability percentage in G2V with one EV.

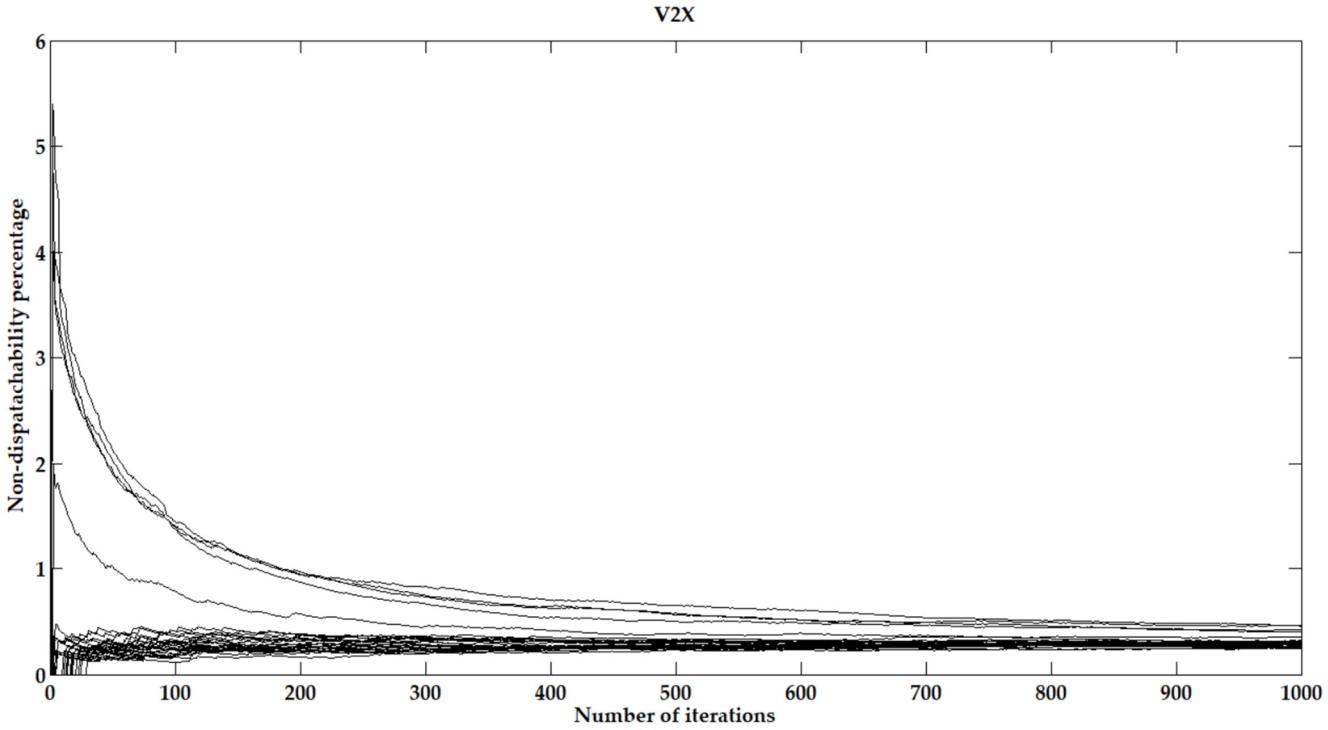

Figure 27. Plot of non-dispatchability percentage in V2X with one EV.

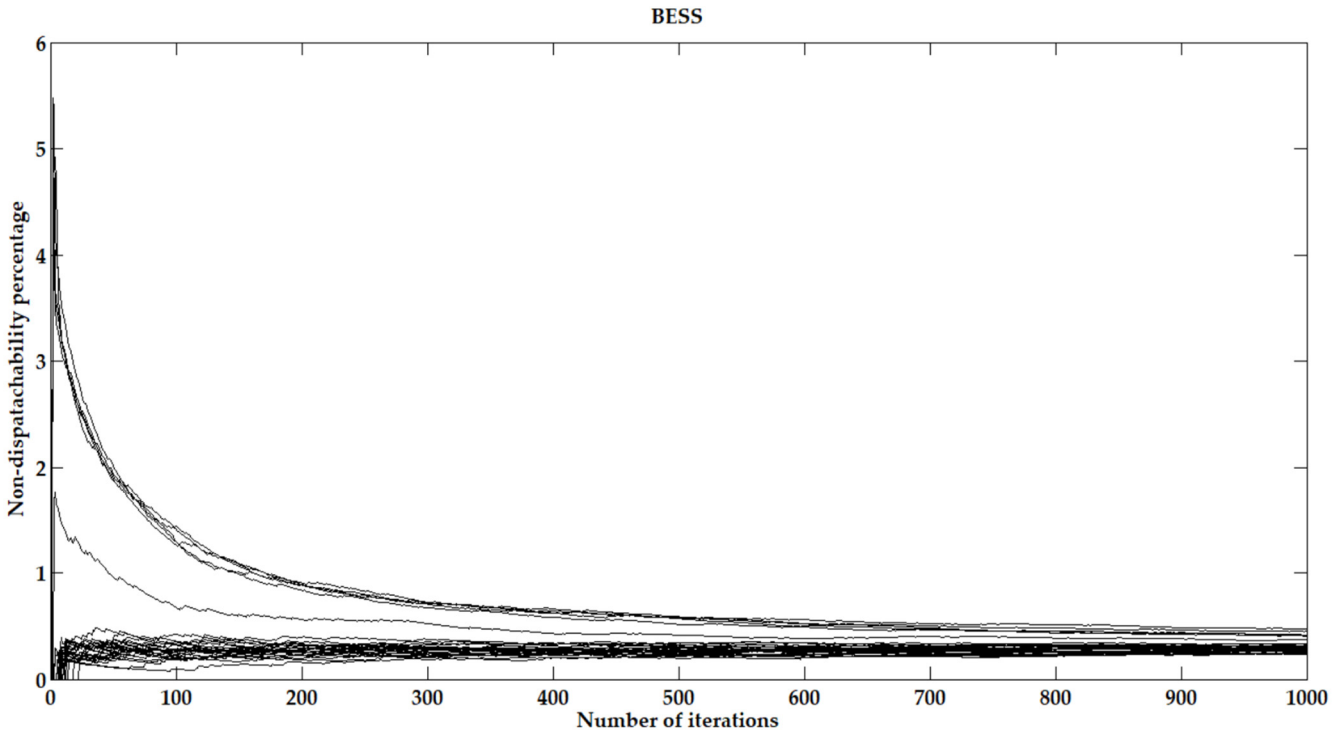

Figure 28. Plot of non-dispatchability percentage in BESS with one EV.

Table 13. Non-dispatchability percentages for thirty runs for G2V, V2X and BESS cases with EV.

Non-Dispatchability (%)			
Seed Count	**G2V (%)**	**V2X (%)**	**BESS (%)**
1	0.2815	0.2931	0.2615
2	0.2588	0.2646	0.2686
3	0.2876	0.2686	0.2428
4	0.2549	0.3529	0.2531
5	0.2803	0.2681	0.2369
6	0.2419	0.3019	0.2704
7	0.237	0.4019	0.2631
8	0.2449	0.2992	0.3529
9	0.3143	0.2943	0.3237
10	0.4127	0.2963	0.3135
11	0.4162	0.3195	0.42
12	0.3691	0.2975	0.2411
13	0.2641	0.282	0.2866
14	0.2677	0.2685	0.2869
15	0.2723	0.2952	0.2621
16	0.3021	0.4222	0.288
17	0.4489	0.4603	0.2464
18	0.2906	0.4571	0.2633
19	0.3276	0.3157	0.2806
20	0.3042	0.2621	0.2797
21	0.3077	0.2477	0.2588
22	0.469	0.2539	0.3312
23	0.251	0.2892	0.3263
24	0.2747	0.2928	0.2857
25	0.2643	0.2815	0.3731

26	0.3035	0.2764	0.2705
27	0.4066	0.2871	0.4026
28	0.2928	0.2855	0.2583
29	0.3349	0.2642	0.2875
30	0.2623	0.2437	0.2774
Mean	0.3081	0.3048	0.2904
SD	0.06361	0.05733	0.04641
Confidence Interval 95%	[0.2844, 0.3319]	[0.2834, 0.3262]	[0.2731, 0.3078]

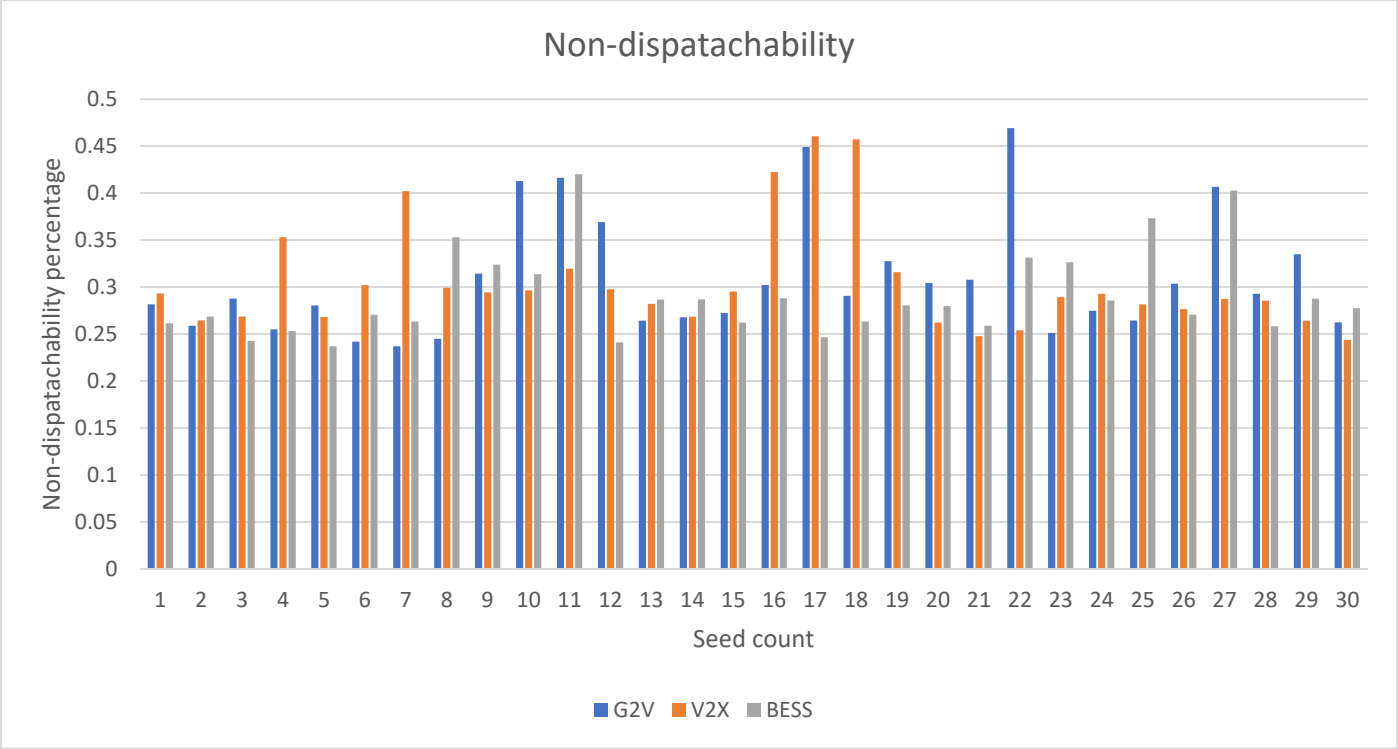

Figure 29. Line plot of non-dispatchability percentages for thirty runs for G2V, V2X and BESS cases with one EV.

Table 14. Summary of non-dispatchability of electric energy supply in G2V, V2X and BESS with one EV.

Grid Non-Dispatchability	G2V	V2X	Stationary BESS
Mean	0.3081%	0.3048%	0.2904%
Standard deviation	0.06361%	0.05733%	0.04641%

4. Discussion

This study quantitatively highlights the benefits of V2X-enabled EVs compared with a baseline case of conventional Grid-to-Vehicle (G2V) charging. To address the challenge of modelling V2X, we first develop a framework in which an EV connects to several bidirectional charging and discharging entities. Such entities include other EVs, infrastructure, load, grid, homes, buildings, devices, etc. All these entities are modelled as nodes having provision of reasonably sized batteries, having battery management systems, bearing intelligent nodes and the ability to dynamically decide timing, extent and assignment of pricing so as to optimize the demand and supply dynamically at each of the nodes throughout the simulation.

4.1. Grid Performance Aspect Comparison

This framework enabled our analytical abilities to evaluate grid parameters, e.g., grid reliability (EIR), non-dispatchability and VRE curtailment in both EV cases. The results are tabulated in Table 15:

Table 15. Summary of impact of G2V, V2X and stationary BESS on grid performance aspects.

EV Count	Grid Aspects	G2V (Reference Case)	V2X	Stationary BESS	Δpp in V2X	Δpp in Stationary BESS
1	Reliability	99.6935%	99.6937%	99.7134%	+0.0002%	+0.0199%
	VRE Curtailment	1.3817%	1.3511%	1.3473%	−0.0306%	−0.0344%
	Non-dispatchability	0.3081%	0.3048%	0.2904%	−0.0177%	−0.0177%
2	Reliability	99.7066%	99.7078%	99.7116%	+0.0012%	+0.0050%
	VRE Curtailment	1.4129%	1.3529%	1.3405%	−0.06%	−0.0724%
	Non-dispatchability	0.3121%	0.3054%	0.3021%	−0.0067%	−0.0100%

Each grid performance-related parameter for a given simulation case is repeated thirty times using an independent seed each time. Furthermore, the experiment is iterated for a thousand times every time.

Simulation results indicate that all three grid performance parameters under consideration gradually improve as we move towards the cases from an islanded microgrid featuring (i) electric vehicles with unidirectional Grid-to-Vehicle charging (G2V), then (ii) electric vehicles featuring vehicle to grid/load/infrastructure/person/building/vehicle/home (V2X), and then to (iii) stationary BESS.

All of these observations remain valid even when the number of EVs was reduced from two to one. This indicates the model clears the sensitivity test with respect to the number of EVs.

There is a subtle difference (<1%), in absolute terms, in the performance-related grid aspects. However, the trend of improvement as we add the V2X feature in conventional EVs and then, alternately, add stationary BESS in the reference case of an isolated microgrid featuring only G2V, is meaningful.

Further, this subtle difference is worth focusing on, as industry-wide performance-related grid parameters are already stable around these percentages of 99% and 1%. Optimizations in the operations of recently added electronic devices will have a less than 1% optimization benefit.

This ABM-based study has resulted in a flexible and modular isolated microgrid model having flexibility to accommodate any parameter of interest in such an analysis.

4.2. Cost Comparison for V2X Versus Stationary BESS

4.2.1. Battery Degradation and Life Cycles

Since this study emphasizes featuring electric vehicles with V2X, it is necessary to compare cost-effectiveness in a microgrid with (i) EVs featuring V2X versus and (ii) equivalently sized stationary BESS in the microgrid.

Both cases are subject to the same handling by the modelled microgrid except for battery degradation, life cycles and battery cost considerations. So, overall comparison of (i) and (ii) is confined to comparison of these three parameters only. Hence, these parameters will be handled outside the general microgrid model and are compared in Table 16.

Table 16. Comparison of battery chemistries and life cycles for stationary BESS and EV [29].

Battery Chemistry	Stationary BESS Cycles	EV Battery Cycles
LFP (Lithium Iron Phosphate)	4000–10,000	2000–5000
NMC (Nickel Manganese Cobalt)	2000–5000	1000–2500
NCA (Nickel Cobalt Aluminum)	2000–4000	1000–2000

In each of the three battery chemistry types, it is observed that the life of a battery is exactly double in terms of charging cycles in the case of stationary BESS. The reason for this is that batteries in EVs are subject to more constraints with respect to thermal stability, DoD, minimum level of charging assurance for ensuring that an EV will remain available for mobility at any time, regenerative braking, etc. This results in an extra burden on managing batteries in an EV. Thus, as Table 16 suggests, the life cycles of batteries in EVs are reduced by roughly 50%, i.e., for a similar environment and battery chemistry, a battery having a life of 4000 cycles in the case of a stationary BESS will have just 2000 charging cycles in an EV. In this study, LFP is chosen as the battery chemistry due to its prevalent use in both cases. Standard battery charging and discharging series resistance–capacitance equations are used while transferring energy in and out of a battery.

It implies that a battery's ageing factor and degradation comparison is depicted by its total number of life cycles.

BESS parameters used in the study are presented in Table 17.

Table 17. BESS parameters [29].

BESS parameters	Value
Chemistry	LFP
Depth of Discharge (DoD)	80%
Cycle-life planning value EFC (Equivalent Full Cycle)	4000–10,000
Daily cycling	1 cycle
Round-trip efficiency	88–92%
Calendar-life planning	10–15 years
End-of-life reference	80% SOH

4.2.2. Cost Considerations

Table 18 presents a comparison of battery costs for stationary BESS and V2X. References [30] and [31] are based on data collected in yet-to-be-peer-reviewed news summaries. Further, the study assumes that the charger, whether unidirectional or bidirectional, is already financed.

Table 18. Cost comparison for V2X versus stationary BESS.

Entity	Stationary BESS	V2X	
Reference	[30]	[31]	
cases	-	Existing G2V retrofit case	New V2G-enabled EV case
Euro cost range	-	€15–50/kWh	€13–43/kWh
USD cost range	73 USD	or 16.73 USD–55.78 USD	or 14.50 USD–47.97 USD
Marginal LFP cost USD	73 USD	36.255 USD	31.235 USD
Life cycles @ SOH	4000	2000	2000
Cost per cycle	1.825 cents	1.81275 cents	1.56175 cents

Since each and every aspect of batteries in stationary BESS and V2X is the same except the number of battery cycles throughout its lifetime, cost per cycle in each of these cases

is sufficient to compare them for overall comparison of battery degradation and cost of battery.

Table 18 clearly shows that V2X offers a more cost-effective alternate of stationary BESS not only in the case of a factory-fitted V2X solution but also in the case of retrofitted case as well.

However, since grid performance parameters perform slightly better in the case of stationary BESS as compared to V2X (no doubt by less than one percentage), it is still worthy to go for a V2X-based long-term energy storage solution. Further, it implies that total time-average parked V2X-featured vehicles' available battery capacity should be subtracted from an intended stationary BESS design for roughly the same microgrid performance.

5. Conclusions

Rapidly changing electrification technologies are becoming prevalent globally. EV charging mechanisms are also evolving at a fast pace. Conventional G2V EV charging systems are being upgraded with V2X charging systems. Further, stationary BESS additions to grids are gaining traction all across the globe. These industry dynamics have motivated this research work.

In this study, a framework is designed to study the flow of energy in an islanded microgrid featuring (i) electric vehicles having Grid-to-Vehicle charging only, (ii) electric vehicles having Vehicle-to-Anything (V2X) and (iii) stationary BESS of size equivalent to EVs in cases (i) and (ii) and removing these EVs.

Such grid performance aspects include reliability, curtailment, and non-dispatchability of electric supply. This study concludes that Vehicle-to-Everything offers benefits, though marginally, over unidirectional charging for all three considered grid performance aspects. Similarly, a stationary Battery Energy Storage System offers benefits, though marginally, over Vehicle-to-Everything for all three grid performance parameters.

The study is repeated for one EV, and the nature of the results remains the same. It implies that the model is validated by the sensitivity test based on the number of EVs.

This study shows (ii) results in 0.0012%, 0.0124% and 0.00111% improvements over (i) and (iii) results in 0.005%, 0.0724% and 0.0045% improvements over (i) in reliability, curtailment and non-dispatchability, respectively, in the case of two EVs.

Similarly, this study shows (ii) results in 0.0002%, 0.0306% and 0.0177% improvements over (i) and (iii) results in 0.0199%, 0.0344% and 0.0177% improvements over (i) in reliability, curtailment and non-dispatchability, respectively, in the case of two EVs.

Further, a cost comparison in (ii) and (iii) is made. It is found that (ii) is a more cost-effective solution, based on yet-to-be-peer-reviewed market research references, than (iii), even if an electric vehicle is retrofitted for Vehicle-to-Everything charging. It implies that the Battery Energy Storage System size requirement in a microgrid is reduced by roughly the equivalent aggregated size of batteries in the same system with Vehicle-to-Everything charging-enabled electric vehicles.

Author Contributions: Conceptualization, M.A.A. and M.A.; methodology, M.A.A., M.A. and A.R.; software, M.A.A.; validation, M.A.A. and A.R.; formal analysis, M.A.A., M.A. and A.R.; investigation, M.A.A. and M.A.; data curation, M.A.A.; writing—original draft preparation, M.A.A. and A.R.; writing—review and editing, M.A.A., M.A. and A.R.; supervision, M.A. and A.R.; project administration, M.A. and A.R. All authors have read and agreed to the published version of the manuscript.

Funding: This research received no external funding.

Institutional Review Board Statement: Not applicable for studies not involving humans or animals.

Informed Consent Statement: Not applicable.

Data Availability Statement: The original contributions presented in this study are included in the article. Further inquiries can be directed to the corresponding author.

Conflicts of Interest: The authors declare no conflicts of interest.

Abbreviations

The following abbreviations are used in this manuscript:

n ϵ N	Set of nodes
$r_{n\text{-}i}$	Tariff of energy at n in its last transaction
r_n^{avg}	Average tariff at n during the last five deals
r_n^{curr}	Current tariff at node n
E_n^{nom}	Nominal SOC level of battery in n
E_n^{gen}	Energy generated in a node
E_n^{min}	Minimum SOC level of battery in n
E_n^{max}	Maximum SOC level of battery in n
E_n^{curr}	Current SOC level of battery in n
E_n^{Δ}	Current nominal tradeable energy of n
E_n^{neigh}	Sum of neighbours' tradeable energy
L_n^{nom}	Nominal load of n
L_n^{min}	Minimum load of n
L_n^{max}	Maximum load of n
L_n^{curr}	Current load of n
E_n^{exim}	Exporter/Importer status of n
E_n^{emer}	NC emergency status of n
E_n^{forc}	Forecasted energy level of a n
ETBT	Expected-To-Be-Transferred energy
C_{curr}	Curtailment evaluated
C_{cum}	Cumulative curtailment
D_{curr}	Non-dispatchability evaluated (in seconds)
D_{cum}	Cumulative non-dispatchability (in seconds)
D_n^{tic}	Timer value at initiation of non-dispatchability at n
D_n^{toc}	Timer value at termination of non-dispatchability at n
D_{cum}^{perc}	Cumulative percentage of non-dispatchability
P_{cum}^{gen}	Cumulative generated energy
P_{cum}	Cumulative energy
α	Demand supply ratio at a node
$t_{cum(s)}$	Cumulative time elapsed (in seconds)

Appendix A

Simulation parameters for each node constitute forty-one parameters for each node. They are grouped as node, nature, rate, energy, load, timings, status, temporary variables, cycles and minimum state of charge values in Table A1. Columns 35–39 are deleted to simplify the table. These five columns comprise five temporary variables used during simulation. Ten nodes of the modelled isolated microgrid and their associated forty-one parameters are displayed in three parts. Publicly shared source code for this isolated microgrid is available at [32].

Table A1. (**a**–**c**) Parameters of ten nodes in the modelled isolated microgrid.

(**a**)

1	2	3	4	5	6	7	8	9	10	11	12
Node	**Nature**	**Rate (USD/kWh)**									
n	n_{nature}	$R_{n,-5}$	$R_{n,-4}$	$R_{n,-3}$	$R_{n,-2}$	$R_{n,-1}$	$R_{n,curr}$	$R_{n,avg}$	$R_{n,range}$	$R_{n,dev}$	$R_{n,perc}$
n	Nature	R_{minus5}	R_{minus4}	R_{minus3}	R_{minus2}	R_{minus1}	$R_{Current}$	$R_{Average}$	R_{Range}	R_{dev}	R_{perc}

1	2	0.14	0.13	0.13	0.13	0.13	0.13	0.132	0.01	0	13
2	0	0.14	0.13	0.13	0.13	0.13	0.13	0.132	0.01	0	13
3	1	0.14	0.13	0.13	0.13	0.13	0.13	0.132	0.01	0	13
4	0	0.14	0.13	0.13	0.13	0.13	0.13	0.132	0.01	0	13
5	2	0.14	0.13	0.13	0.13	0.13	0.13	0.132	0.01	0	13
6	0	0.14	0.13	0.13	0.13	0.13	0.13	0.132	0.01	0	13
7	2	0.14	0.13	0.13	0.13	0.13	0.13	0.132	0.01	0	13
8	0	0.14	0.13	0.13	0.13	0.13	0.13	0.132	0.01	0	13
9	2	0.14	0.13	0.13	0.13	0.13	0.13	0.132	0.01	0	13
10	0	0.14	0.13	0.13	0.13	0.13	0.13	0.132	0.01	0	13

(**b**)

13	**14**	**15**	**16**	**17**	**18**	**19**	**20**	**21**	**22**
Energy (kWh)									
$E_{n,nom}$	$E_{n,min}$	$E_{n,max}$	$E_{n,range}$	$E_{n,curr}$	$E_{n,\Delta}$	$E_{n,dev}$	$E_{n,perc}$	$E_{n,prosumed}$	$E_{n,target}$
E_{Nom}	E_{Min}	E_{Max}	E_{Range}	E_{Curr}	E_{Delta}	E_{Dev}	E_{Perc}	$E_{Prosumed}$	E_{Target}
0.25	0	0.5	0.5	0.4	0.15	0.15	0.8	0	0
0.5	0	1	1	0.6	0.1	0.1	0.6	0	0
1	0	2	2	1.4	0.4	0.4	0.7	0	0
1	0	2	2	1.6	0.6	0.6	0.8	0	0
0.75	0	1.5	1.5	0.75	0	0	0.5	0	0
20	0	40	40	20	0	0	0.5	0	0
1.25	0	2.5	2.5	1.22	−0.03	−0.03	0.488	0	0
35	0	70	70	69	34	34	0.986	0	0
0.25	0	0.5	0.5	0.48	0.23	0.23	0.96	0	0
1.5	0	3	3	0.15	−1.35	−1.35	0.05	0	0

(**c**)

23	**24**	**25**	**26**	**27**	**28**	**29**	**30**	**31**	**32**	**33**	**34**	**40**	**41**
Load (Watt)							**Timings (s)**			**Status**		**Cycles**	**MinSOC**
$L_{n,nom}$	$L_{n,min}$	$L_{n,max}$	$L_{n,range}$	$L_{n,curr}$	$L_{n,dev}$	$L_{n,perc}$	tic_n	toc_n	Δt_n	$busy_n$	$exim_n$	Cycles	MinSOC
L_{Nom}	L_{Min}	L_{Max}	L_{Range}	L_{Curr}	L_{Dev}	L_{Perc}	Tic	Toc	DeltaT	Busy	Exim	Cycles	MinSOC
15	10	45	35	22	7	0.62857	0	0	0	0	1	0	20
30	15	60	45	20	−10	0.44444	0	0	0	0	1	0	20
50	20	80	60	72	22	1.2	0	0	0	0	1	0	20
50	20	70	50	50	0	1	0	0	0	0	1	0	20
45	10	90	80	12	−33	0.15	0	0	0	0	1	0	20
1000	100	2000	1900	1200	200	0.63157	0	0	0	0	1	0	20
80	5	150	145	124	44	0.85517	0	0	0	0	0	0	20
1800	250	3200	2950	2400	600	0.813559	0	0	0	0	1	0	20
15	2	35	33	31.5	16.5	0.954545	0	0	0	0	1	0	20
100	45	150	105	133	33	1.266667	0	0	0	0	0	0	20

References

1. Manbachi, M.; Ordonez, M. Intelligent agent-based energy management system for islanded AC–DC microgrids. *IEEE Trans. Ind. Inform.* **2020**, *16*, 4603–4614.
2. Almada, J.B.; Leão, R.P.S.; Almeida, R.G.; Sampaio, R.F. Microgrid distributed secondary control and energy management using multi-agent system. *Int. Trans. Electr. Energy Syst.* **2021**, *31*, e12886.
3. Al-Ismail, F.S. DC microgrid planning, operation, and control: A comprehensive review. *IEEE Access* **2021**, *9*, 36154–36172.
4. Ali, S.; Zheng, Z.; Aillerie, M.; Sawicki, J.P.; Pera, M.C.; Hissel, D. A review of DC microgrid energy management systems dedicated to residential applications. *Energies* **2021**, *14*, 4308.
5. Jirdehi, M.A.; Tabar, V.S.; Ghassemzadeh, S.; Tohidi, S. Different aspects of microgrid management: A comprehensive review. *J. Energy Storage* **2020**, *30*, 101457.
6. Elmouatamid, A.; Ouladsine, R.; Bakhouya, M.; El Kamoun, N.; Khaidar, M.; Zine-Dine, K. Review of control and energy management approaches in micro-grid systems. *Energies* **2020**, *14*, 168.
7. Fontenot, H.; Dong, B. Modeling and control of building integrated microgrids for optimal energy management—A review. *Appl. Energy* **2019**, *254*, 113689.
8. Rana, M.J.; Rahi, K.H.; Ray, T.; Sarker, R. An efficient optimization approach for flexibility provisioning in community microgrids with an incentive-based demand response scheme. *Sustain. Cities Soc.* **2021**, *74*, 103218.

9. Xie, P.; Jia, Y.; Chen, H.; Wu, J.; Cai, Z. Mixed-stage energy management for decentralized microgrid cluster based on enhanced tube model predictive control. *IEEE Trans. Smart Grid* **2021**, *12*, 3780–3792.
10. Shen, S.; Haider, S.I.; Habeeb, R.; Fitzek, F.H.P. Coordinating Day-Ahead and Intraday Scheduling for Bidirectional Charging of Fleet EVs. *Automation* **2025**, *6*, 64. https://doi.org/10.3390/automation6040064.
11. Harasis, S.; Sozer, Y.; Elbuluk, M. Reliable islanded microgrid operation using dynamic optimal power management. *IEEE Trans. Ind. Appl.* **2021**, *57*, 1755–1766.
12. Criollo, A.; Benavides, D.; Arévalo, P.; Minchala-Avila, L.I.; Morales-Jadan, D. Enhancing Grid Stability in Microgrid Systems with Vehicle-to-Grid Support and EDLC Supercapacitors. *Batteries* **2025**, *11*, 231. https://doi.org/10.3390/batteries11060231.
13. Jeong, H.; Kim, J. Optimal Operation Strategy of Virtual Power Plant Using Electric Vehicle Agent-Based Model Considering Operational Profitability. *Sustainability* **2025**, *17*, 11291. https://doi.org/10.3390/su172411291.
14. Khan, M.W.; Wang, J.; Xiong, L. Optimal energy scheduling strategy for multi-energy generation grid using multi-agent systems. *Int. J. Electr. Power Energy Syst.* **2021**, *124*, 106400.
15. Khan, W.; Wang, J. Multi-agents based optimal energy scheduling technique for electric vehicles aggregator in microgrids. *Int. J. Electr. Power Energy Syst.* **2022**, *134*, 107346.
16. Chang, Z.; Liu, X.; Zhang, Q.; Zhang, Y.; Wang, Z.; Zhang, Y.; Li, W. Consideration of Wind-Solar Uncertainty and V2G Mode of Electric Vehicles in Bi-Level Optimization Scheduling of Microgrids. *Energies* **2025**, *18*, 823. https://doi.org/10.3390/en18040823.
17. Finecomess, S.A.; Gebresenbet, G.; Zada, W.Y.; Mulugeta, Y.; Addisie, A. Optimization of Vehicle-to-Grid, Grid-to-Vehicle, and Vehicle-to-Everything Systems Using Artificial Bee Colony Optimization. *Energies* **2025**, *18*, 2046. https://doi.org/10.3390/en18082046.
18. Ru, J.; Gillott, M.; Shipman, R. Vehicle-to-Grid (V2G) Research: A Decade of Progress, Achievements, and Future Directions. *Energies* **2025**, *18*, 6148. https://doi.org/10.3390/en18236148.
19. Waseem, M.; Sreeshobha, E.; Shashidhar Reddy, K.; Donateo, T. State-of-the-Art and Advancement of Charging Infrastructure in Electric Mobility: An Integrated Review. *Energies* **2024**, *17*, 6137. https://doi.org/10.3390/en17236137.
20. Veza, I.; Syaifuddin, M.; Idris, M.; Herawan, S.G.; Yusuf, A.A.; Fattah, I.M.R. Electric Vehicle (EV) Review: Bibliometric Analysis of Electric Vehicle Trend, Policy, Lithium-Ion Battery, Battery Management, Charging Infrastructure, Smart Charging, and Electric Vehicle-to-Everything (V2X). *Energies* **2024**, *17*, 3786. https://doi.org/10.3390/en17153786.
21. Lin, F.-J.; Lu, S.-Y.; Hu, M.-C.; Chen, Y.-H. Stochastic Optimal Strategies and Management of Electric Vehicles and Microgrids. *Energies* **2024**, *17*, 3726. https://doi.org/10.3390/en17153726.
22. Waldron, J.; Rodrigues, L.; Deb, S.; Gillott, M.; Naylor, S.; Rimmer, C. Exploring Opportunities for Vehicle-to-Grid Implementation through Demonstration Projects. *Energies* **2024**, *17*, 1549. https://doi.org/10.3390/en17071549.
23. Khezri, R.; Steen, D.; Anh Tuan, L. Willingness to Participate in Vehicle-to-Everything (V2X) in Sweden, 2022—Using an Electric Vehicle's Battery for More Than Transport. *Sustainability* **2024**, *16*, 1792. https://doi.org/10.3390/su16051792.
24. Garcia-Torres, F.; Baez-Gonzalez, P.; Tobajas, J.; Vazquez, F.; Nieto, E. Cooperative optimization of networked microgrids for supporting grid flexibility services using model predictive control. *IEEE Trans. Smart Grid* **2021**, *12*, 1893–1903.
25. Lu, K.; Dong, S.; Song, Y. A distributed economic power dispatch strategy considering state of charge for microgrids. *IEEE Access* **2025**, *13*, 66276–66289.
26. Correia, A.F.M.; Goncalves Neves, M.A.; Casal Dos Reis, A.I.; Coimbra, A.P.; De Oliveira De Almeida, T.R.; Moura, P.; De Almeida, A.T. Architecture and operational control for resilient microgrids—A university case study. *IEEE Access* **2025**, *13*, 51373–51387.
27. Techbriefs. My Opinion: Why Microgrids? 2026. Available online: https://www.techbriefs.com/component/content/article/49929-my-opinion-why-microgrids (accessed on 23 September 2026).
28. U.S. Department of Energy. FOTW #1356, August 19, 2024: Household Vehicles Were Parked 95% on a Typical Day in 2022. 2022. Available online: https://www.energy.gov/cmei/vehicles/articles/fotw-1356-august-19-2024-household-vehicles-were-parked-95-typical-day-2022 (accessed on 5 November 2026).
29. Viswanathan, V.; Mongird, K.; Franks, R.; Li, X.; Sprenkle, V.; Pacific Northwest National Laboratory. *Grid Energy Storage Technology Cost and Performance Assessment*; Publication No. PNNL-33283; U.S. Department of Energy: Washington, DC, USA, 2022.
30. NEIAAP. Battery storage system prices continue to fall sharply, BNEF and Ember reports find. 2025. Available online: https://www.neiaap.com/article/battery-storage-system-prices-continue-to-fall-sharply-bnef-and-ember-reports-find (accessed on 23 September 2026).

31. Koloch, J.; Brödel, M.; Bussieweke, F.; Götz, K.; Seidenfus, M.; Winkler, T.; Grosu, C.; Lienkamp, M. Costs and parameters of BEV electrification: A comprehensive review of battery system innovations, vehicle-level integration, and energy system synergies. *npj Clean Energy* **2026**, *2*, 28. https://doi.org/10.1038/s44406-026-00044-6.
32. Google Drive. Code. 2026. Available online: https://docs.google.com/document/d/1qhHC5NVozkEIZeESqVOYY1SfKfrnQq2u/edit (accessed on 18 November 2026).

Disclaimer/Publisher's Note: The statements, opinions and data contained in all publications are solely those of the individual author(s) and contributor(s) and not of MDPI and/or the editor(s). MDPI and/or the editor(s) disclaim responsibility for any injury to people or property resulting from any ideas, methods, instructions or products referred to in the content.